Photophysics of Tryptophan Fluorescence: Link with the Catalytic Strategy of the Citrate Synthase from *Thermoplasma acidophilum*†

Linda C. Kurz,*,‡ Brett Fite,‡ John Jean,‡ Jung Park,‡ Tim Erpelding,§ and Patrik Callis§

Department of Biochemistry and Molecular Biophysics, Division of Biology and Biomedical Sciences, Washington University School of Medicine, St. Louis, Missouri 63110, and Department of Chemistry and Biochemistry, Montana State University, Bozeman, Montana 59717

Received August 5, 2004; Revised Manuscript Received October 31, 2004

ABSTRACT: The formation of all major intermediates in the reaction catalyzed by the citrate synthase from *Thermoplasma acidophilum* is accompanied by changes in tryptophan fluorescence. The largest change is the strong quenching observed on formation of the binary complex with substrate, oxaloacetate (OAA). The four tryptophan residues present in the enzyme have been changed to nonfluorescent ones in various combinations without major perturbations in protein stability, enzyme mechanism, or other physical properties. W348, residing in the hydrophobic core of the protein behind the active site wall ca. 9 Å from OAA, is responsible for the majority of the protein's intrinsic fluorescence and all of the quenching that accompanies OAA binding. Lifetime studies show that all of the quenching results from excited-state processes. The lack of solvent isotope effects on the quantum yields excludes a quenching mechanism involving proton transfer to an acceptor. There are no significant changes in fluorescence properties in single site mutants of residues near W348 that change conformation and/or interactions when OAA binds. This result excludes these changes from a direct role. Electron transfer from the indole excited state to some acceptor is the major quenching mechanism; the reduced quenching observed in the 5F-W-substituted protein strengthens this conclusion. Using the X-ray structures of the unliganded enzyme and its OAA binary complex, hybrid quantum mechanics−molecular dynamics (QM-MM) calculations show that OAA itself is the most likely quencher with the OAA carbonyl as the electron acceptor. This conclusion is strengthened by the ability of an α-keto acid model compound, trimethylpyruvate, to act as a diffusional quencher of indole fluorescence in solution. The theoretical calculations further indicate that the positive electrostatic potential surrounding the OAA carbonyl within the enzymes' active site is essential to its ability to accept an electron from the excited state of W348. These same environmental factors play a major role in activating OAA to react with the carbanion of acetyl-CoA. Since carbonyl polarization plays a role in the catalytic strategies of numerous enzymes whose reactions involve this functional group, tryptophan fluorescence changes might be useful as a mechanistic probe for other systems.

Citrate synthase (EC 4.1.3.7) catalyzes condensation between the carbonyl of oxaloacetate (OAA)[1] and the acetyl methyl of the thioester, acetyl-coenzyme A (AcCoA).[1] The initial product of the condensation, *S*-citryl-CoA (CitCoA),[1] is hydrolyzed in a second step to the eventual products, citrate and CoA (Scheme 1). Despite an apparent conflict in the requirements for efficient catalysis of the ligase and hydrolase reactions of citrate synthase, both steps take place within the same active site and utilize the same catalytic residues (*16*, *17*).

Citrate synthase is a prototype system for enzyme mechanisms, illustrating several of the important strategies utilized by biological catalysts. Consequently, it has been the subject of numerous structural (*18*−*20*) and kinetic studies (*5*, *7*, *17*, *21*, *22*). Citrate synthase uses substrate destabilization (*5*, *21*) to increase reactivity of the electrophilic center through polarization of the OAA carbonyl (Scheme 2). It catalyzes the kinetically and thermodynamically difficult proton transfer from a carbon acid (*23*, *24*), the methyl group of AcCoA, to the carboxylate side chain of the active site aspartate residue (Scheme 2). The enzyme stabilizes the

† Supported by National Institutes of Health Grant GM33851 (L.C.K. and B.F.), NSF Grant MDB-0133064 (P.C. and T.E.), and ACS-PRF Grant AC6-36506 (J.J.). Support for B.F. was provided in part by a grant to Washington University from the Howard Hughes Medical Institute through the Undergraduate Biological Sciences Education Program.

* To whom correspondence should be addressed: e-mail, kurz@biochem.wustl.edu; phone, 314-362-3401; fax, 314-362-7183.

‡ Washington University School of Medicine.

§ Montana State University.

[1] Abbreviations: AcCoA, acetyl-coenzyme A; CCS, citrate synthase from chicken heart; CD, circular dichroism; CitCoA, *S*-citryl-coenzyme A; CMCoA, carboxymethyl-coenzyme A; CMX, carboxymethyldethiacoenzyme A; cMDH, cytoplasmic malate dehydrogenase from pig heart; dethiaAcCoA, dethiaacetyl-coenzyme A; DsCS, psychrophilic CS from an antarctic bacterium; CT, charge transfer state; DTNB, 5,5′-dithiobis-(2-nitrobenzoic acid); OAA, oxaloacetate; FRET, Förster resonance energy transfer; PCS, citrate synthase from pig heart; PfCS, citrate synthase from *Pyrococcus furiosus*; QM-MM, hybrid quantum mechanics−molecular dynamics; NATA, *N*-acetyltryptophanamide; SAS, saturated ammonium sulfate solution; TIM, triosephosphate isomerase; TMP, trimethylpyruvate; TpCS, citrate synthase from *Thermoplasma acidophilum*; WT, TpCS with no mutations; TM, W245F-W115F-W17F TpCS (TpCS containing only one W residue, W348).

10.1021/bi048323l CCC: $30.25
Published on Web 01/13/2005

Scheme 1: Citrate Synthase Reaction

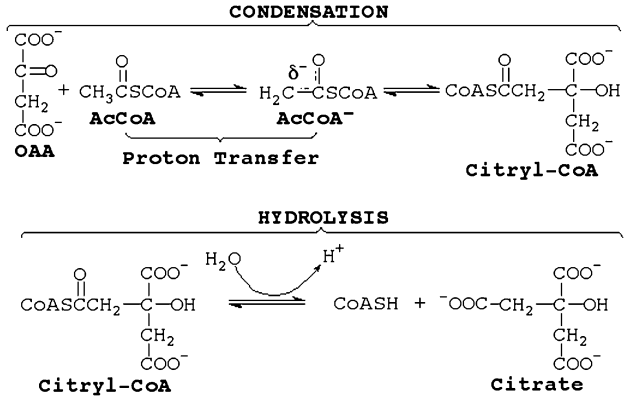

Scheme 2: Formation of a New Carbon−Carbon Bond between the Methyl Carbanion of AcCoA and the Carbon of the Polarized OAA Carbonyl

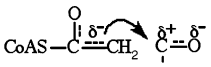

resulting nucleophilic carbanion/enolate (*25*−*27*) (Scheme 2) that is the reactive species condensing with the OAA carbonyl to form the new C−C bond of citrate.

Citrate synthase provides one of the clearest examples of the roles of protein flexibility and changes in macromolecular conformation as necessary components of a catalytic machine (*18*, *28*, *29*). Turnover cannot occur without them (*16*) as crystal forces are sufficient to lock the protein conformation and prevent reaction (crystals have no activity). The details of the conformational transitions that accompany turnover have been the subject of several theoretical analyses (*30*−*32*). At the beginning of the reaction cycle, the active site is in an open conformation, accessible to substrates (products) and solvent. Starting with the binding of OAA (the first substrate to bind in the preferred-ordered kinetic mechanism), the enzyme undergoes successive conformation changes so that the active site becomes increasingly solvent inaccessible until the final products, CoA and citrate, are formed, at which time the process is reversed and products are released to the solution. The covalent bond-making/breaking events of both the condensation and hydrolysis steps (Scheme 1) take place buried deep within the protein where the active site and its contents are buried about 15 Å from the solvent-accessible surface (*19*, *20*, *33*). The stable intermediate, *S*-citryl-CoA (CitCoA), is never released to the solution (*34*).

While a great deal of structural and kinetic data are available for the enzymes from both eukaryotic and prokaryotic organisms, the most completely characterized system is the enzyme from the thermophilic Archaeon, *Thermoplasma acidophilum* (TpCS)[1] (*3*, *7*). TpCS has the convenient and unusual property that essentially every chemical and conformational intermediate has a different fluorescence spectrum or quantum yield (vide infra) greatly facilitating kinetic studies.

Protein intrinsic tryptophan fluorescence changes such as those observed in TpCS have frequently been exploited as probes to obtain kinetic and equilibrium data for a large number of processes of biochemical interest, including ligand binding, substrate turnover, and protein folding/unfolding. Many incisive studies have established that intrinsic quenching of Trp fluorescence in proteins is usually caused by photoinduced electron transfer (ET) in which an electron is transferred from the indole ring to a nearby amide of the peptide backbone; we will consider other possibilities such as proton transfer and internal conversion, but they will be ruled out by experimental and theoretical data, vide infra (*36*−*44*). This belief in the ET mechanism is strongly reinforced by the observation that the fluorescence quantum yield for the 3-methylindole (devoid of amides) is nearly independent of environment over the range from hydrocarbon to water, being near 0.3 in all cases (*45*). Every Trp in a given protein experiences a unique environment and structural relation to nearby amides, and electron transfer rates are known to generally exhibit the requisite sensitivity to structure and environment. The precise reason for the remarkable environmental sensitivity of the quenching rate of Trp in proteins (over 30-fold) is still unsettled. Recently, a step toward realizing the potential for detailed structural and electrostatic information in the intensity variations has largely been made in the form of QM-MM simulations that show how electron transfer to the somewhat unlikely electron acceptor amide can be semiquantitatively estimated from the electric field strength and direction caused by local charged and polar groups (*46*−*48*). We now report a detailed analysis of tryptophan photophysics for TpCS in structural and electrostatic terms that have even added mechanistic insights; we propose that the substrate OAA is the likely electron acceptor as a consequence of the unusual active site environment of this enzyme.

In this work we will present experimental and theoretical analyses of the structural and mechanistic bases of the TpCS fluorescence changes that accompany the formation of the various chemical intermediates and substrate complexes with particular emphasis on the TpCS−OAA binary complex. TpCS contains four tryptophan residues in each subunit of the homodimer at sequence positions 17, 115, 245, and 348. Using a series of single and multiple site-directed mutant enzymes, we attribute the observed fluorescence changes to the tryptophan residue(s) responsible. W348, buried behind the wall of the active site, is found to be solely responsible for the strong fluorescence quenching observed in the OAA−TpCS binary complex. Hybrid quantum mechanics−molecular dynamics (QM-MM) calculations (*46*−*48*) are applied to predict fluorescence wavelengths, lifetimes, and quantum yields.

The most significant (and surprising) result is that the strong quenching of W348 fluorescence appears to be another consequence of polarization of the OAA carbonyl that occurs in the enzyme's active site and that is an essential part of its catalytic strategy (*5*, *21*). Just as this polarization enhances the reactivity of the carbonyl carbon toward condensation with the negatively charged carbanion of AcCoA (Scheme 2), it has also enhanced the ability of OAA to accept an electron from the excited state of W348, thereby efficiently quenching its fluorescence. The calculations suggest that the large positive electrostatic potential surrounding the OAA carbonyl is essential to its ability to accept electron transfer from the excited state of indole. This same positive electrostatic potential is part of the means by which the enzyme increases the OAA carbonyl's reactivity toward the AcCoA carbanion. As carbonyl polarization is believed to be essential to the reactions of many enzymes' catalyzing reactions involving this functional group (*49*−*53*), tryptophan fluo-

Table 1: Primers Used for the Construction of TpCS Mutants[a]

mutant	forward primer	reverse primer	restriction enzyme
W17F	5′-GC AAA GGG CT***c*** GAG GAT GTC AAT ATA AAG Ttc ACA AGG CTC AC-3′	5′-GT GAG CCT TGT gaA CTT TAT ATT GAC ATC CTC ***g***AG CCC TTT GC-3′	*Xho*I
W115F	5′-CA AAG TTC AAG Ttt AAC AAG GAT ACG GAC AGA GAC GTT GCA G-3′	5′-C TGC AAC GTC TCT GTC CGT ATC CTT GTT aaA CTT GAA CTT TG-3′	*Mse*I
W245F	5′-G ATA AAG GAT CCC GC***a*** ATG GTG GAG AAG Ttc TTC AAC GAC AAC-3′	5′-GTT GTC GTT GAA gaA CTT CTC CAC CAT ***t***GC GGG ATC CTT TAT C-3′	*Nco*I
W348F	5′-GCG CT***c*** TC***g*** AGG GTT ACA GGG Ttc CAG GCA CAC TTC ATA G-3′	5′-C TAT GAA GTG TGC CTG gaA CCC TGT AAC CCT ***c***Ga ***g***AG CGC-3′	*Xho*I
W348Y	5′-GG GTT ACA GGG Tac CAG GCA CAC TTC ATA GAG-3′	5′-CTC TAT GAA GTG TGC CTG gtA CCC TGT AAC CC-3′	*Ban*I
R344K	5′-TC TTC GCG CTA TCC AaG GTT ACA GGG TGG CA-3′	5′-TG CCA CCC TGT AAC CtT GGA TAG CGC GAA GA-3′	*Eco*RII
R344M	5′-TC TTC GCG CTA TCC AtG GTT ACA GGG TGG CA-3′	5′-TG CCA CCC TGT AAC CaT GGA TAG CGC GAA GA-3′	*Eco*RII
H187Q	5′-CTC TAC ACA GAC CAg GAG GTG CCT GCA TC-3′	5′-GA TCC AGG CAC CTC cTG GTC TGT GTA GAG-3′	*Bst*NI
H262Q	5′-GAC TCA TGG GCT TT***t*** GGC CAg AGG GTA TAC AAG-3′	5′-GT CTT GTA TAC CCT cTG GCC ***a***AA GCC CAT GAG-3′	*Bal*I
H222Q	5′-GT CCG CTG CAg GGC GGT GCA GC-3′	5′-GC TGC GCC GCC cTG CAG CGG AC-3′	*Msl*I

[a] Bases changed are indicated as lower case letters. Single underlining denotes the amino acid changed. Boldface italic letters indicate bases changed to introduce a silent mutation and a new restriction site for the enzyme indicated in the last column.

rescence may be able to provide another mechanistic probe toward our understanding of this important enzymic catalytic strategy.

MATERIALS AND METHODS

Enzymes and Mutants. Mutants listed in Table 1 were constructed in plasmid pRec7-ArCS (*7*) using the QuikChange mutagenesis kit by Stratagene. In addition to the base changes required for the desired residue change (indicated by lower case and a single underline in the table), a silent mutation (indicated by lower case boldface italic) was sometimes included to introduce a new restriction site to produce a unique fragment size after plasmid digestion. That restriction enzyme is indicated in the last column of the table. A silent mutation was not introduced when the mutation producing the desired amino acid change simultaneously introduced the new restriction site (restriction enzyme listed in the last column). After PCR, the mutagenized DNA was used to transform the supercompetent *Escherichia coli* strain XL1-Blue supplied with the kit. Candidate colonies were identified by their ability to grow on LB−carbinicillin plates. A liquid culture of single colonies was grown, glycerol stocks were prepared for storage, and the plasmid DNA was isolated. The plasmid DNA (prepared with the EndoFree Plasmid Maxi kit by Qiagen) was digested with the indicated restriction enzyme. Agarose gel electrophoresis confirmed the presence of the predicted restriction fragments unique to the mutation as well as the correct plasmid size. In most cases, the entire TpCS gene was then sequenced to ensure that no other changes had been introduced inadvertently. The verified maxiprep DNA was then used to transform the expressing strain, MG1655. In several cases, plasmid DNA was also isolated and sequenced from the expressing strain. Prior to protein preparation, cells from glycerol stocks were plated on a carbinicillin plate and single colonies used for liquid starter cultures. In the case of W245F, the mutant with unusually high activity, its molecular weight measured by electrospray mass spectrometry confirmed the substitution of a single F for W.

Plasmid Puc19 containing S192A TpCS was a generous gift of Drs. C. R. Thompson and Michael Danson of the University of Bath, U.K. This plasmid DNA was also used to transform the vigorous strain MG1655 for enzyme expression. However, since this plasmid constitutively expresses the protein, no induction was required for enzyme preparation.

The general outline of protein preparations was that described in ref *7*. However, the affinity resin previously used (Dyematrex Gel Red A; Millipore Corp.) is no longer manufactured. For some enzymes (WT,[1] R344K, W348F, W245F, W17F, W115F) we successfully substituted the Sigma Reactive Red 120−agarose resin that contains the chemically identical dye ligand and a dye content of 5−9 μmol/mL. The mutant containing three F substitutions, W245F, W115F, W17F TpCS (TM),[1] binds inconveniently tightly to this high dye content resin. (Protein could be eluted only by solutions containing high concentrations of OAA/CoA or urea, making recovery of the ligand-free or native enzyme difficult or impossible.) However, Sigma Reactive Red 120 resin type 3000-CL containing only 3−5 μmol/mL dye allowed about 33% recovery of the pure TM mutant enzyme with elution by the usual salt gradient. Mutant W348Y failed to bind to the original Dyematrex Gel Red A resin but could be successfully purified by affinity chromatography using high dye content Sigma Reactive Red 120 resin. In general, we observed that samples with lower 280/260 ratios bind poorly to the dye resin. Passing such samples over a HiTrap Q HP (Pharmacia) FPLC column equilibrated in 20 mM Tris buffer and 0.1 mM EDTA, pH 8.0, removes highly negatively charged contaminants such as polynucleotides and some other protein contaminants and improves subsequent binding to the dye column, yield, and final purity. TpCS is positively charged at pH 8.0 [pI = 8.9 (*7*)] and does not bind to the HiTrap resin.

Substrates and Inhibitors. CMCoA and CitCoA were prepared as described in refs *25*, *27*, and *54* except that diafiltration was used to desalt and concentrate the fractions after chromatography on DEAE-Sepharose Fast-Flow (110−

160 μequiv/mL). Diafiltration and concentration were accomplished with use of a cellulose acetate 500 MW cutoff membrane (YC05; Amicon) in a pressurized stirred dialysis cell equipped with a reservoir containing water (CMCoA) or 1 mM H(D)Cl (CitCoA). DethiaAcCoA was obtained from Dr. Dale Drueckhammer. CD_3AcCoA was prepared by the reaction of acetic-d_6 anhydride (Aldrich) with an excess of CoA according to ref *55* and purified as for CMCoA and CitCoA. Trimethylpyruvic acid (TMP)[1] was the product of ChemPacific Corp.

Enzyme concentrations and extinction coefficients at 280 nm for W mutants were calculated from the absorbances at 280 nm of solutions whose concentrations[2] have been determined by active site (stoichiometric) titrations of the TpCS−OAA complexes (*27*) with the very tight binding inhibitor, CMCoA.[1] The TpCS−OAA complexes (conditions for saturation with OAA were determined separately by fluorescence titration, vide infra) were titrated by monitoring the CD signal at 260 nm as described previously (*7*).

Solutions for all physical measurements have the reported pH ± 0.02 pH units and the reported temperatures ±0.1 °C.

Kinetic Methods and Substrate Concentrations. Absorbance data were collected using a Cary 3 spectrophotometer. Concentrations of AcCoA, OAA, and CitCoA were measured enzymatically using PCS[1] or TpCS. CoA concentrations were measured using a DTNB[1] assay and compared to concentrations measured by absorbance at 260 nm to check for oxidation. Only CoA samples whose concentrations determined by both methods agreed within a few percent were used for experiments. Oxidation of CoA was prevented by purging solutions with argon gas and conducting experiments under an argon gas blanket in cases where changing CoA concentrations could affect results. Citrate synthase activities with the normal substrates, OAA and AcCoA, or with the intermediate, CitCoA, were measured as described previously (*7*). CitCoA lyase activity was measured by detecting OAA production through its reduction to malate by NADH (monitored at 340 nm) catalyzed by a large excess of sMDH[1] (*7*). Kinetic constants for mutant enzymes (K_m's, k_{cat}s, substrate isotope effects, partition ratios) were all determined as described previously for WT (*7*).

Circular Dichroism. Spectra and titration data were collected using a Jasco J-715 spectropolarimeter and analyzed as described previously (*22*).

Isoelectric focusing was done on a PhastGel electrophoresis system (Pharmacia) using dry gels reconstituted in narrow range ampholyte mixtures. The most consistent results were obtained using a pH gradient (nominal pH 7.0−10) together with a chemical spacer (arginine). PhastGel Dry IEF gels were rehydrated in 2 mL of water, 300 μL of glycerol, 3.0 mg of arginine, 100 μL of Pharmalyte, pH 8.0−10.5, and 60 μL of Ampholine, pH 7−9. The chemical spacer, arginine, has the effect of flattening the pH gradient in the region of its pK_a, ca. 9, where we desired increased resolution of the TpCS mutants. Isoelectric focusing conditions were those suggested by the manufacturer (Pharmacia Separation technique file, 101). Samples were applied to the middle of the gel, the acidic end, or both to ensure that focus had been achieved. Isoelectric points were determined by comparison with the positions of proteins in the high p*I* standards kit (Amersham Biosciences) containing 10 proteins (p*I* 5−10.4). We resolved the identity of minor bands in the standards by using pure proteins (Sigma). Protein bands were stained by Coomassie Brilliant Blue R with the addition of 0.1% w/v $CuSO_4$ to decrease background. Determinations of p*I* were reproducible to ∼0.05 pH unit.

Steady-State Fluorescence Spectroscopy. Spectra and titration data (using time base parameters) were obtained using a PTI Alphascan spectrofluorometer with a thermostated cell compartment and cell stirrer. Excitation and emission wavelengths and other instrument parameters are included in Results where appropriate. Solutions containing high concentrations of OAA required corrections for inner filter effect because the enol form of OAA that comprises 5−7% of the material in solution has a long wavelength tail with significant absorption at the excitation wavelengths.[3] Only very high OAA concentrations (>5 mM) required an additional inner filter correction on emission wavelengths. The corrections are minimized by using short path length cells in the excitation beam whenever possible. Correction factors are obtained by titrating both the buffer and solutions of *N*-acetyltryptophanamide (NATA)[1] with the same OAA concentrations that are added to the protein samples. We used front face fluorescence data collection (22.5° to the incident beam) for solutions with very high absorbance and requiring large inner filter effect corrections (H187Q−OAA).

We are able to obtain the spectrum of the TpCS−CitCoA complex during its hydrolysis. Because the binding of the CitCoA intermediate to the enzyme is very much tighter than other substrates or products, the major enzyme form present during steady-state hydrolysis of CitCoA is the CitCoA−TpCS complex. Judicious choice of concentrations of enzyme and CitCoA substrate resulted in sufficient complex lifetime (10−12 s) and signal so that, together with reduction of the spectral width and time dwell, we were able to obtain a noisy spectrum of the complex. Reported spectra with acceptable signal to noise ratios are averages of three to four repetitions.

OAA Dissociation Constant Determinations. OAA dissociation constants were determined by fluorescence titrations as reported previously (*7*).

Quantum Yield Determinations. Quantum yield is defined as

$$Q = Q_R \frac{I}{I_R} \frac{OD_R}{OD} \frac{n^2}{{n_R}^2} \quad (1)$$

Q and Q_R are the quantum yield of the sample and reference (W in water), I and I_R are the integrated intensities of the sample and reference, OD and OD_R are the optical densities of the sample and reference at the excitation wavelength,

[2] Enzyme concentrations are given in terms of active sites (not the dimer).

[3] At the excitation wavelength of 295 nm we estimate the extinction coefficient for an α-carboxylic acid carbonyl from the spectrum of TMP (cannot enolize) as about 23 M^{-1} cm^{-1}. OAA solutions exhibit absorbances at this wavelength equivalent to 289 M^{-1} cm^{-1}, and we conclude that the enol extinction coefficient at 295 nm is the difference, 266 M^{-1} cm^{-1}. A 10 mM OAA solution such as might be desired for diffusion quenching studies has an absorbance of 2.9, beyond the range where corrections are reliable with conventional instrument configurations. Even though only the keto form is an enzyme substrate, the presence of the enol form does not interfere with enzyme assays because the enol−keto conversion is rapid on the time scales of all our experiments (*1*).

and n and n_R are the refractive indices of the sample and reference solutions (*56*, *57*). Both emission and excitation instrument corrections were applied. (We thank Dr. Timothy Lohman for use of his PTI spectrofluorometer that had recently been calibrated with a NIST standard lamp.) The largest uncertainty in these quantum yield measurements arises because of the necessity of using an excitation wavelength of 295 nm to avoid exciting Y residues. TpCS contains 19 Y residues (*58*) that contribute to the emission spectrum at exciting wavelengths lower than 295 nm. The TpCS emission spectra have wavelength emission maxima that are quite blue (λ_{max} of 315 nm), and thus we cannot observe a significant portion of the blue edge of the emission spectrum using a 295 nm excitation wavelength. To calculate the quantum yield, we estimated the unobservable areas of the protein spectra by obtaining the emission spectrum using lower exciting wavelength (280 nm), normalizing the maxima, and in the case of W348Y applying a minor 1−2 nm wavelength shift. The normalized spectra obtained with 280 nm excitation were used to estimate the missed area. The normalized spectra with different excitation wavelengths for WT and TM were nearly superimposable, suggesting that Y makes only a small contribution for these proteins. For W348Y, a more pronounced red shift was noted for 295 nm excitation in comparison with 280 nm excitation. The normalized spectrum from WT was used with a 1.5 nm shift to estimate the blue edge of the emission spectrum for the W348Y mutant.

Time-Resolved Fluorescence Spectroscopy. Picosecond fluorescence decay measurements were carried out using the time-correlated single photon counting method (Becker & Hickl SPC-630 PC board). The laser system was a 76 MHz mode-locked Ti:S laser (Coherent Mira 900F) pumped by a diode-pumped Nd:YVO_4 laser (Coherent Verdi V10). The excitation (300 nm, vertically polarized) was obtained by frequency tripling the Ti:S fundamental (U-Oplaz Technologies). The excitation beam (~500 μW) was focused onto the sample using a 50 mM quartz lens. The emission was collected by a 60 mm lens, passed through a polarizer oriented at the magic angle, and focused onto a photomultiplier tube (PMT; Hamamatsu 5773P-03) with a 75 mm lens. A 400 nm short-wave pass filter was used to reject residual fundamental and second harmonic beams, and a 345 nm high pass filter was used to block the water Raman line. Due to the unusually small Stokes' shift in these proteins, only the red edge of the fluorescence spectrum was collected. The anode pulse of the PMT provided the start pulse for the TAC, and the stop pulse was obtained by splitting off ~10% of the excitation beam and focusing it onto a UV-sensitive Si:C photodiode (JEC 0.1). The full width at half-maximum of the instrument response function, determined using the light scattered by a dilute solution of nondairy coffee creamer, was ~170 ps. Samples were contained in a 1 cm × 1 cm quartz cuvette thermostated at 20 °C. Sample concentrations were 5 μM for the TpCS mutants. Freshly prepared solutions of OAA were added in sufficient amounts to result in complete complexation. For each sample, decay curves were collected using 2048 channels (6.10 ps per channel) and terminated when 2^{16} counts were obtained in the peak channel. The buffer fluorescence decay (including OAA) was then measured for an equivalent collection time for subtraction prior to analysis. Buffer fluorescence counts typically accounted for ~4−6% of the total counts. All experiments were done in duplicate.

Time-resolved fluorescence quenching experiments were carried out using 8 μM NATA with acrylamide or trimethylpyruvate (TMP) as the quencher. Background subtractions were accomplished as described above by measuring the decay of buffer solutions containing the appropriate concentration of quencher.

Fluorescence Decay Analysis. Decay curves were analyzed by a standard nonlinear least squares, iterative reconvolution algorithm (based on the Simplex method) using the Center for Fluorescence Spectroscopy (CFS) software package (available at http://cfs.umbi.umd.edu) assuming a discrete sum of exponentials decay law according to the equation:

$$I(t) = \sum_i \alpha_i e^{-t/\tau_i} \tag{2}$$

where τ_i and α_i are the time constants and corresponding amplitudes, respectively. From the fitted parameters, the amplitude-weighted lifetimes were determined according to the equation:

$$\langle \tau \rangle_{amp} = \frac{\sum_i \alpha_i \tau_i}{\sum_i \alpha_i} \tag{3}$$

Bimolecular quenching constants, k_q, were determined using the equation:

$$\frac{\tau_0}{\tau} = 1 + k_q \tau_0 [Q] \tag{4}$$

where τ and τ_0 are the lifetimes of NATA in the absence and presence of quencher (Q), respectively.

QM-MM Fluorescence Quantum Yield Calculations. Fluorescence quantum yields and lifetimes were estimated using a hybrid QM-MM method, recently applied to predicting Trp fluorescence wavelengths (*46*) and fluorescence quantum yields (*47*, *48*) from electrostatics.

Briefly, the QM part is Zerner's INDO/S-CIS method (*59*) as modified to include the local electric field and potentials. The MM part is Charmm (version 26b) (*60*). The QM part may be one of two options. The first includes the entire W residue and the C-terminal amide of the preceding residue, capped with hydrogens so that the QM part is *N*-formyltryptophanamide (NFTA). The second option is to include a second residue or a ligand along with the W. In the latter option, the two residues are treated by the QM as a supermolecule of independent molecules. This option can identify electron transfer to a site not part of the W and its amides. A QM calculation is performed every 10 fs during an MD trajectory on a system consisting of all protein atoms (H added to a crystal structure) and about 6500 explicit waters. The ^1L_a (fluorescing) and lowest charge transfer (CT) state energies are recorded (as modified by the electric potentials arising from all atomic point charges of the protein and water). The CT states may be described as resulting from the excitation of an electron from a donor molecular orbital (MO) to an empty MO on the acceptor, creating a "radical ion pair". This is treated as an excited singlet state, and the

supermolecule approach automatically includes the Coulombic interaction of the "radical pair" and relaxations about these charges.

The electron densities on the QM molecule are updated in the Charmm database, and the trajectory is resumed. The electron transfer rate constant is estimated using a Fermi rule-based electron transfer theory:

$$k_{ET} = \frac{2\pi}{\hbar}V^2(2\pi\sigma^2)^{-(1/2)}\int \rho_{FC}(\Delta E_{00})e^{-(1/2)((\Delta E_{00}-\langle\Delta E_{00}\rangle)/\sigma)^2}\,d\Delta E_{00} \quad (5)$$

where V is the quantum mechanical electronic coupling matrix element ("interaction") connecting the initial fluorescing state with the CT state and ρ_{FC} is the density of final vibronic states in the CT state that are degenerate with the initial (fluorescing state), which is a function of the separation in 0-0 transitions, ΔE_{00}, for the removal of an electron from the donor (indole ring) and the capture of an electron by the acceptor (amide or ligand). The integral averages over a Gaussian distribution of ΔE_{00} values, with σ the standard deviation of the fluctuation of ΔE_{00} about its mean,[4,5] $\langle\Delta E_{00}\rangle$. $\langle\Delta E_{00}\rangle$ and σ are the mean and variance of the QM $^1L_a-CT$ transition energies found in the QM-MM trajectories. The trajectories are short (10 ps) relative to the fluorescence lifetime, so it is assumed here that there are not longer term fluctuations that could lead to heterogeneity in rate. Because there is no simple way to estimate the electronic coupling matrix element with confidence, V was taken as one constant fitting variable, and a second fitting variable was an additive constant, D, to the semiempirical $\langle\Delta E_{00}\rangle$. The two constants coming from the best fit for 24 Trps in 17 proteins were $V = 10\ cm^{-1}$ and $D = -4000\ cm^{-1}$ (*48*). As an ad hoc starting point, the same constants and ρ_{FC} were applied to OAA in this study, although they are not formally transferable. The OAA bond lengths in the CT state involving electron transfer from W to OAA were obtained from a B3LYP/3-21G ab initio Gaussian 98 (*61*) calculation on the OAA radical anion (charge $= -3$), wherein a partial optimization was performed fixing the bond angles and dihedrals to match those of the crystal structures.[6] Further details regarding the method are described elsewhere (*47*, *48*).

RESULTS AND DISCUSSION

The first step toward understanding the changes in the protein's intrinsic fluorescence that occur upon formation of the various substrate and intermediate complexes is the preparation of mutant proteins with W residues substituted by nonfluorescent residues with minimal perturbations in protein structure, stability, and catalytic and ligand binding properties. We first prepared proteins with single phenylalanine substitutions for each tryptophan as indicated in Table 1. The proteins W17F, W115F, and W245F are obtained in yields comparable to WT; W348F is obtained in lower yield. When stored at 4 °C, the enzymatic activities of 2−4 μM protein solutions of WT, W17F, W115F, and W245F remain unchanged for at least 48 h. W348F is unstable. While W348F can be purified to a single band on SDS−PAGE gels and some experiments performed, its activity decreases to zero within a few days even when stored at 50 mg/mL. Rational design[4] successfully predicts Y as a stable substitution for W at residue 348; W348Y is stable and obtained in high yields. We prepared double and triple F substitutions starting with W245F and finally ending with W17, 115, 245F (TM) that contains the single W residue at position 348. The double and triple mutants are stable and active.

The three proteins, WT, TM, and W348Y, were used extensively for fluorescence measurements and theoretical calculations. Although there are some subtle changes, their catalytic mechanisms are closely similar. Their kinetic constants are compared in Table 2. Their OAA K_D's are compared in Table 3. Isoelectric focusing gels are shown in panels A (W245, 17, 115F, WT) and B (W348Y) of Figure 1.

All three W-modified proteins have fundamentally the same chemical mechanism as WT. The macroscopic kinetic

[4] We sought the source of *importance of W348 to protein stability* and are able to identify W348 interactions that might contribute to the stability of the free enzyme and its OAA complex, respectively. Using the CaPTURE program (*2*) and the structure of the free enzyme (*3*), a strong cation−π interaction between W348 and R344 may contribute up to −5 kcal/mol to protein stability of each subunit. Analyzing the OAA complex similarly, we find that this cation−π interaction is lost in the OAA complex because R344 rotates and forms two hydrogen bonds with the 1-carboxylate of OAA (Figure 7). In the OAA complex, the indole N of W348 also participates in a new hydrogen bond with the alcoholic side chain hydroxyl of S192. S192 is a residue conserved in all known citrate synthases. These new hydrogen bonds, as well as other interactions of OAA, probably compensate for the loss of the cation−π interaction between W348 and R344. Increased stabilities of WT[1] and mutant protein−OAA complexes (*4*) and of OAA itself (*5*) upon formation of the binary enzyme−OAA complex have been well documented previously. Of course, W348F cannot form an H-bond with S192. Without a crystal structure, it is impossible to be certain of the exact cause of instability of W348F. Using SWISS-Pdb Viewer (*6*) to model this substitution, we found it possible to substitute F for W without causing any clashes in the free enzyme structure, but the cation−π stability averaged over both subunits (−1.8 kcal/mol) is significantly less favorable than the original interaction with W and falls a little short of the conventional cutoff for a significant interaction (*2*). The OAA complex models are more problematic since all four subunits in the asymmetric unit have slightly different structures. Substitution of F for W at residue 348 caused a clash with R344 in one subunit and a modestly favorable cation−π interaction worth −2.8 kcal/mol stabilization in the other. Without a more sophisticated analysis or a crystal structure of the mutant, the exact cause of the instability of W348F is uncertain. By modeling other candidate substitutions, however, we identified W348Y as a potentially stable substitution. In the model of the free enzyme, the oxygen of the phenol side chain of 348Y can form an H-bond with the oxygen of the side chain of S192 as well as a cation−π interaction with R344 worth −3.7 kcal/mol. These rough estimates are apparently a valid qualitative guide as W348Y is both stable and active. Design of a nonperturbing substitution for R344, the other member of the cation−π pair, is particularly problematic in the present case since this residue provides two hydrogen bonds to the 1-carboxylate of OAA in the complex (Figure 7). Using Swiss-PDB viewer to model the substitutions of K or M for R344, we observed that it was possible for a K residue at 344 to form one hydrogen bond with the OAA 1-carboxylate. Rotamers with no clashes are possible with both K and M substitutions. R344K is stable and active at saturating substrate concentrations.

[5] The relationship between ΔE_{00} and σ and the more commonly used free energy change (ΔG_0) and reorganization energy (λ) is that $\sigma^2 = 2\lambda k_B T$ and $\Delta E_{00} = \Delta G_0 + \lambda$.

[6] Russell et al. (*3*) supplied us with the apoenzyme coordinates. We are grateful to Rupert Russell, Michael Danson, and Garry Taylor for providing us with the coordinates of the binary OAA complex prior to their publication. Obtaining higher resolution structures of the apoenzyme and several of these complexes are a high priority in our laboratories as such structures will provide the basis for more complete theoretical calculations.

Table 2: Kinetic Constants of TpCS W Mutants[a]

enzyme	k_{cat}^{AcCoA} (min^{-1})	K_m^{OAA} (μM)	K_m^{AcCoA} (μM)	k_{cat}^{CitCoA} (min^{-1}) (ratio)[b]	K_m^{CitCoA} (μM)	partition ratio[c] v_i^r/v_i^f	substrate isotope effect[d] ${}^{D}k_{cat}^{CD_3AcCoA}$
WT	588	3.0	0.67	686 (1.17)	<1	0.040	1.07
TM (W245, 115, 17F)[e]	924	3.0	3.6	1040 (1.13)	0.7	0.064	1.13
W348Y	404	3.0	0.85	465 (1.15)	0.5	0.040	1.13
R344K	870	370	17				
H187Q	660	54	10	760 (1.15)	0.5	0.02	

[a] All kinetic constants were determined in 50 mM EPPS buffer and 0.1 mM EDTA, pH 8.00, at 20 °C. Uncertainties in kinetic constants from replicate measurements are less than 5%. K_m's are reproducible between different protein preparations to about 20%. k_{cat}s are more variable with 30% differences observed occasionally between preparations. Substrate isotope effects are reproducible to about 2%. [b] Ratio of k_{cat} with substrate CitCoA to that with AcCoA/OAA; monitors degree to which the hydrolysis step is rate-determining (*7*). [c] The partition ratio with CitCoA as substrate is the initial velocity to produce reactants OAA and AcCoA divided by initial velocity to produce products Cit and CoA; monitors internal thermodynamics. [d] This notation is a convention of isotope effect chemists and is translated as the "apparent" (as opposed to intrinsic effect on a single elementary step) deuterium isotope effect on the k_{cat} kinetic constant (a complex function of elementary step rate constants) with CD_3AcCoA as the isotope-containing substrate with the deuterium label in the methyl group. [e] TpCS containing three F substitutions for W17, W115, and W245. Only W348 remains.

Table 3: Absolute and Relative Quantum Yields of TpCS, Various Mutants, and Their OAA Complexes

protein	K_D^{OAA} (μM)	absolute quantum yield[a] (relative to W in water)	relative quantum yield of OAA complex compared to unliganded protein[d]	relative $\langle\tau\rangle_{amp}$[e] complex/free
TpCS WT	1.3	0.15 (1.09)	0.50 (0.48, pH 7, 200 μM OAA) (0.44, 10 mM OAA) (0.54, 10 mM OAA + 100 μM CMCoA)[f]	0.52
TM	1.2	0.27 (1.99)	0.21 ± 0.05 (pH 8) 0.19 (pH 7) 0.23 (pH 9)	0.16
TM in D_2O buffer[b]	nd[c]	1.10 (relative to H_2O buffer)	0.22	nd
W348Y	0.9	0.08 (0.55)	1.15	1.09
H222Q	33	nd	0.37	nd
H262Q	42	nd	0.51	nd
H187Q	~600	nd	0.62 (10 mM OAA) 0.58 (10 mM OAA + 100 μM CMCoA)	nd
S192A	1.8	nd	0.39	nd
R344K	~1100	nd	~0.6 (5K_D, pH 8) 0.53 (pH 7)	nd
R344M	>10 mM (not saturatable)	nd	<0.7	nd

[a] Excitation was at 295 nm. The absolute quantum yield of W in water was taken as 0.14 (*57*). [b] Buffers are 50 mM EPPS and 0.1 mM EDTA, pH or pD 8.00, in H_2O or D_2O, respectively. [c] nd = not determined. [d] Relative quantum yields for OAA complexes were determined by the relative areas from 305 to 420 nm of the unliganded enzyme and the complex. Comparison of single mutants in H or R residues should be made with WT because these mutations contain all four W residues. [e] Determined from lifetime studies. See Table 4 for absolute values of this parameter calculated according to eq 3. [f] Absolute quantum yields of TpCS solutions and their OAA complexes are a little sensitive to ionic strength and the nature of the anion. Solutions to which 25 mM KCl or 10 mM Na_2SO_4 has been added have reduced fluorescence by a few percent with the dianion somewhat more effective. This salt effect probably contributes to the apparent quenching in complexes studied by front face fluorescence at high (10 mM) OAA concentrations.

constants (k_{cat}s and K_m's) are very similar. They have the same rate-determining step for the overall k_{cat}, CitCoA hydrolysis. This is shown by the observation that the k_{cat}s with the intermediate CitCoA as substrate are only slightly greater (15%) than those starting with AcCoA/OAA (*7*). The partitioning of the stable intermediate (the ratio of the initial rates that CitCoA goes either forward to products or back to reactants) is an especially sensitive indicator of the internal thermodynamics; these values are very similar for all three mutants (*17*). The apparent CD_3AcCoA substrate isotope effect (the extent to which the intrinsic primary isotope effect for the proton transfer from the methyl of AcCoA is expressed in the k_{cat} for the overall reaction) and changes in this value are other sensitive indicators of any changes in the values of rate constants for elementary steps within and leading from the central complex. In the present case, given the absence of changes in the nature of the overall slow step, changes in the value of this isotope effect would reflect alterations in the rate of production of the AcCoA enolate relative to the rate of its subsequent condensation with OAA. Since all three proteins have about the same substrate isotope effect, this is another indication that there are no major changes in the internal rate constants.

There are some subtle mechanistic differences between the W-modified proteins. The trend in k_{cat} values, TM > WT > W348Y with AcCoA/OAA as substrates, has been replicated over several preparations. The same trend is evident in the k_{cat} for CitCoA as expected since the hydrolysis reaction remains the slow step for all three enzymes. The other kinetic constants of all three proteins are closely similar except for the K_m of AcCoA for TM, which is 3−4 times greater than that of the other three proteins. K_D's of other CoA analogues are also higher for the TM mutant (data not shown).

Figure 1 shows isoelectric focusing gels for the W (as well as some other) mutants. TM has a p*I* ~0.2 higher than the WT, and this may be related to the larger K_m for AcCoA for this mutant (Table 2). W17F also has a p*I* ~0.2 higher than WT. W17 is part of a short stretch of β-sheet (residues 16−18) whose hydrogen-bonding partners (residues 368′−370′)

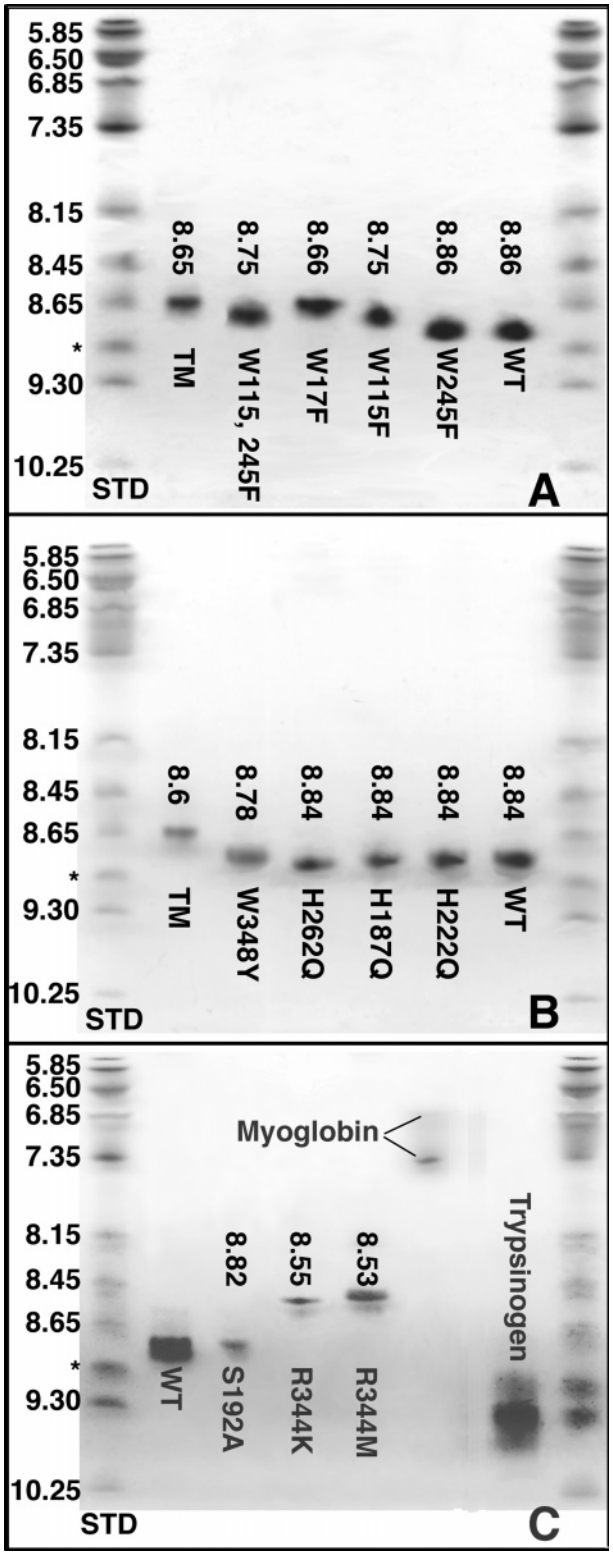

FIGURE 1: Isoelectric focusing gels. Panel A: lanes 1 and 8 (from left to right), high p*I* standard (Amersham Biosciences); lane 2, TM; lane 3, W115, 245F; lane 4, W17F; lane 5, W115F; lane 6, W245F; lane 7, WT. The band marked with as asterisk is commonly present in trypsinogen and is present when the Sigma IEF standard is examined alone (panel C). Panel B: lanes 1 and 8 (from left to right), high p*I* standard; lane 2, TM; lane 3, W348Y; lane 4, H262Q; lane 5, H187Q; lane 6, H222Q; lane 7, WT. Panel C: lanes 1 and 8 (from left to right), high p*I* standard; lane 2, WT (overloaded); lane 3, S192A; lane 4, R344K; lane 5, R344M; lane 6, myoglobin p*I* standard (Sigma); lane 7, trypsinogen p*I* standard (Sigma). Focusing in the gel in panel C was not quite complete as indicated by some faint smearing and doubling of bands.

arise from the other subunit of the dimer. W115F has a p*I* ~0.1 higher than WT. W115 is located in the large domain with no obvious important role. The p*I* value for W348Y is increased less than 0.1 pH unit. No changes at all are evident for the p*I* of W245F. The p*I* changes resulting from individual W to F mutations are not additive in TM. The observed p*I* changes for W mutants are not as large as that caused by changing the full charge in an obligatorily positive residue to an obligatorily neutral side chain. Thus, the p*I* of R344M (panel C) is raised 0.33 unit over that of WT. (Interestingly, the p*I* of R344K is closer to R344M than to WT and probably indicates that this K residue is neutral in the unliganded enzyme.) We conclude that the p*I* changes in W mutants represent only subtle pK_a changes that do not affect the catalytic mechanism or protein structure in any significant way. Thus, we are free to use these mutants for mechanistic and spectroscopic studies with only minor caution.

Steady-State Fluorescence Spectroscopy: Every Conformational and Chemical Intermediate in the Citrate Synthase Reaction of TpCS Has a Unique Emission Spectrum or Quantum Yield. The emission spectra of TpCS WT, W17-115-245F (TM), and W348Y and of their binary and ternary complexes with several substrates, products, intermediates, and intermediate analogues are shown in Figure 2.

Note the strong quenching of fluorescence that accompanies formation of the OAA binary complex in WT and TM. An enhancement occurs when the OAA complex forms with W348Y. Thus the quenching observed in WT and TM is attributable to W348. All of the ternary complexes containing OAA are strongly quenched, including the OAA−CoA abortive complex (not shown), except for the OAA−dethiaAcCoA complex (a subject of subsequent work). All of the complexes in W348Y show enhancement over the free enzyme. Accordingly, the relative quenching shown by the TM−OAA binary complex is greater than it is in WT−OAA since the other tryptophan residues whose fluorescence yields are enhanced with OAA binding are not present.

The shoulder to the high-wavelength side of the spectrum of WT and TM can also be attributed to the single residue, W348, since it is absent in the spectrum of W348Y but present in TM spectra.

Comparisons of similar fluorescence data (not shown) from the appropriate single F mutants show that both W348 and W245 contribute to the enhancement that occurs when the substrate analogue, dethiaAcCoA, binds to the OAA complex. The slight enhancement observed in the WT spectrum when the complex forms between the enzyme, OAA, and CMCoA (an analogue of AcCoA enolate) is attributable to W115 (data not shown).

These fluorescence changes have proven indispensable in disentangling the kinetic constants into rate constants for elementary steps in the mechanism. Those results are the subjects of subsequent reports. This report concentrates on the physical basis of the fluorescence changes induced by OAA binding in terms of protein structure and environment including both experimental and theoretical results.

Absolute Quantum Yields. The emission spectra of the three proteins along with that of W in water that we used to determine the quantum yields are shown in Figure 3. The absorbances of samples were carefully matched at the excitation wavelength, 295 nm. The unobservable parts of

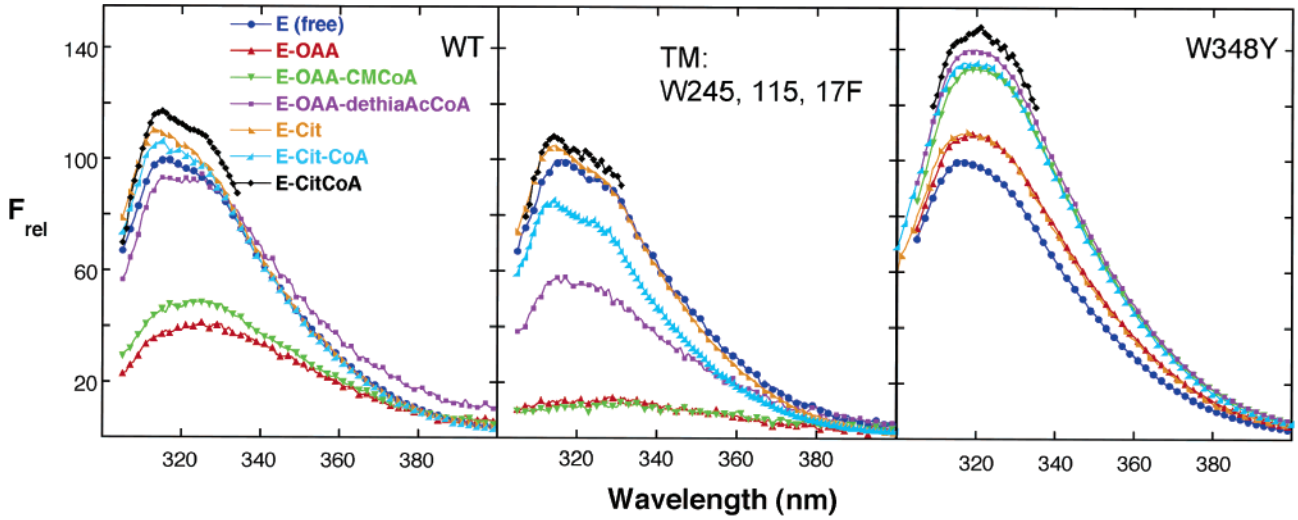

FIGURE 2: Fluorescence emission spectra of WT (left panel), TM (W245, 115, 17F) (middle panel), and W348Y (right panel) and their complexes with substrates, products, intermediates, and intermediate analogues: free enzymes, blue; OAA binary complex, red; OAA−CMCoA enolate analogue ternary complex, green; OAA−dethiaAcCoA ternary complex, lilac; citrate binary complex, orange; citrate−CoA product complex, light blue; CitCoA stable intermediate complex, black. The fluorescence spectra of all three proteins were normalized to that same protein in the absence of ligands with a value of 100 assigned to the fluorescence at their emission wavelength maxima (315 nm) to emphasize the effects of complexation with ligands (see Figure 3 and Table 3 for absolute quantum yields).

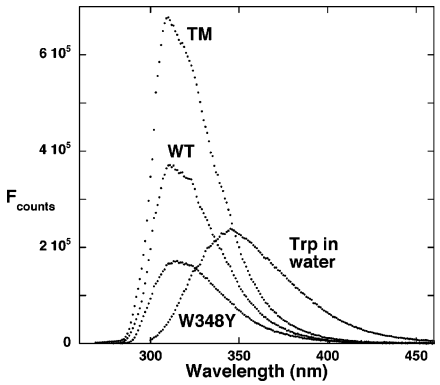

FIGURE 3: Emission spectra of TM, WT, W348Y, and Trp in water used to determine absolute quantum yields. Samples had matched optical densities at 295 nm.

the spectra were reconstructed as described in Materials and Methods. Table 3 compares these quantum yields along with relative quantum yield data for the OAA complexes of several other mutants. The absolute quantum yield of W348, which dominates the emission of WT, is about twice that of tryptophan in solution (Table 3 and Figure 3).

Time-Resolved Fluorescence. The presence of multiple tryptophans (with the exception of the TM and TM−OAA), together with the intrinsic conformational heterogeneity of the W side chain, results in highly nonexponential decays for most proteins. The TM and its OAA complex require only two components to obtain an adequate fit (as judged by the χ^2 criterion), whereas the other mutants and their OAA complexes require three components. Addition of a fourth exponential to the decay model did not result in a significant improvement in the fit. The fractional amplitudes, time constants, amplitude-weighted average lifetimes, and χ^2 values for each mutant and its corresponding OAA complex are shown in Table 4. Each protein decay is found to contain both subnanosecond and nanosecond decay components, which measurably change on complex formation. In all cases, subnanosecond components with time constants comparable

Table 4: Fluorescence Decay Parameters for W Citrate Synthase Mutants and Their OAA Complexes

sample	α_1	α_2	α_3	τ_1 (ns)	τ_2 (ns)	τ_3 (ns)	χ^2	$\langle\tau\rangle_{amp}$ (ns)
WT	0.37	0.25	0.38	0.17	1.04	3.70	1.67	1.74
WT−OAA	0.43	0.28	0.29	0.15	0.97	1.98	1.56	0.91
TM		0.18	0.82		0.68	4.29	2.10	3.64
TM−OAA	0.75	0.13	0.12	0.10	0.91	3.43	1.44	0.60
W348Y	0.20	0.20	0.40	0.18	0.93	2.28	1.56	1.13
W348Y−OAA	0.32	0.34	0.34	0.20	1.16	2.26	1.42	1.23

to the instrument response were obtained. These components account for 20−∼50% of the decay. To test the ability of the fitting algorithm to accurately determine the parameters for these components, simulated decays composed of three exponentials with amplitudes and time constants representative of those in Table 4 and containing Poisson random noise were generated and convoluted with the experimental instrument response function. Analysis of these simulated curves showed that these fast components could be determined within ∼10%. The agreement between the relative $\langle\tau\rangle_{amp}$s and relative quantum yields shown in Table 3 is also consistent with our view that the short components are recovered reasonably accurately.

For the single W-containing TM, 82% of the decay is contained in a 4 ns component. The remaining 18% of the amplitude is contained in a short (0.23 ns) component, illustrating that the W348 side chain, though buried in the densely packed protein core behind the active site, does experience some conformational heterogeneity. The presence or absence of a nearby water molecule hydrogen bonding to the adjacent amide can have a large effect on quantum yield and might be responsible for the heterogeneity observed in the decay of unliganded TM. The average excited-state lifetime of the TM decreases substantially upon formation of the OAA complex. The measured decay curves (upper panel) and the residuals from the nonlinear least squares analyses (lower two panels) for these two species are shown in Figure 4. The dotted line is the instrument response

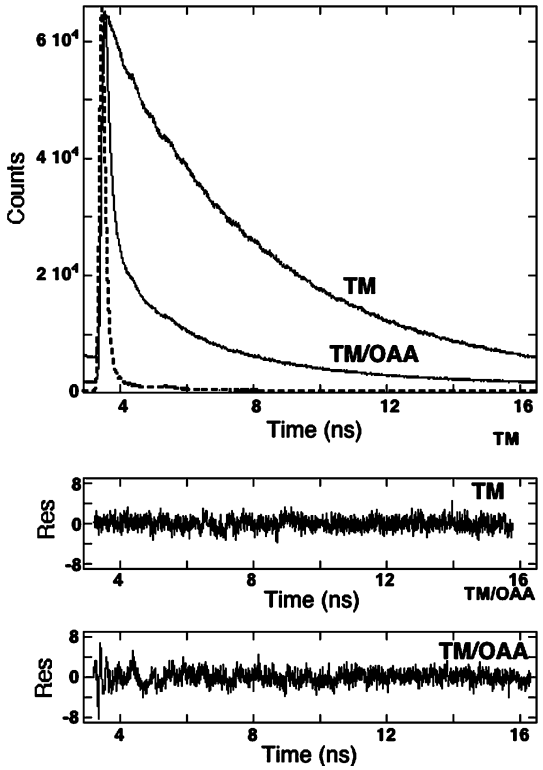

FIGURE 4: Fluorescence decay of TM and its OAA complex. The residuals correspond to the fit for the complex. The dotted line is the instrument response function.

function. As is evident from the residuals for the TM/OAA complex, the fit is not perfect over the first few hundred picoseconds. Addition of a third exponential did not result in a measurable overall improvement in the residuals. This may indicate the presence of decay components considerably faster than our resolution. Since we are only observing the red-most edge of the emission, such components might arise, for example, from rapid, small amplitude reorganization of the local protein environment. If such amplitudes are present, then the average lifetime reported for the OAA complex in Table 4 represents an upper limit to the true value.

Decay parameters for all of the proteins studied are shown in Table 4. The observation that 75% of the decay of the TM−OAA complex is contained in a 100 ps component clearly illustrates the dynamic nature of the quenching process in this complex. If the quenching process is purely dynamic in nature, then the ratio of the fluorescence quantum yields (obtained from the steady-sate measurements) in the presence and absence of OAA should be directly proportional to the ratio of the average excited-state lifetimes. For TM, $\phi_{complex}/\phi_{free} = 0.19$ and $\langle\tau\rangle_{complex}/\langle\tau\rangle_{free} = 0.16$, confirming that excited-state reaction(s) is (are) responsible for the strong quenching in this protein complex. As shown in Table 3, reasonably good agreement is also obtained for WT and W348Y, establishing the dynamic nature of the quenching in these proteins as well.

W348 dominates the WT fluorescence. Though there is in general no one-to-one correspondence between discrete decay components and specific Ws in WT and the W348Y mutant, it is evident from comparing the data for the unbound proteins in Table 4 that the long component in WT derives primarily from W348. Formation of WT−OAA results in a ~48% reduction in the average lifetime (compared to 50% reduction seen in the steady-state yield), which is consistent with the substantial quenching of this W as seen in the TM. Also consistent with the steady-state measurements is the enhancement of the fluorescence from W348Y in the OAA complex. The average lifetime increases 9% upon complexation and the steady-state quantum yield by 15%.

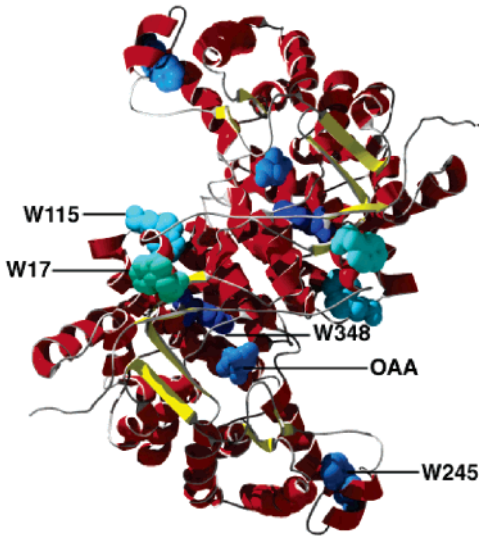

FIGURE 5: Ribbon diagram of TpCS−OAA (A and B subunits) with W residues and OAA space-filled and colored by solvent accessibility. This figure was constructed using the SWISS-Pdb viewer (*6*), available at http://www.expasy.org/spdbv/, and then rendered by POV-Ray ray tracer, available at http://www.povray.org/.

The time-resolved results clearly demonstrate that the presence of OAA leads to efficient deactivation of the excited state of W348 in each of these proteins and reveals the approximate time scale (~100 ps) of this process. The rapid time scale of the nonradiative deactivation of the W excited state makes this process amenable to hybrid QM-MM simulations as will be discussed below.

Understanding the Fluorescence of W Residues in TpCS and the Sensitivity of Their Quantum Yields and Lifetimes to the Occupants of the Active Site. In the past, changes in protein intrinsic fluorescence that accompany the binding of ligands have been ambiguously attributed to "conformation changes". If more detailed explanations of fluorescence changes are offered, they are most commonly attributed to changes in solvent exposure (particularly if accompanied by a shift in wavelength of the emission maximum) or the change in position of a quencher (arising either from the side chain of a nearby residue or from solvent). These common explanations can be excluded as causing the quenching of W348 fluorescence that accompanies the binding of OAA (vide infra).

A ribbon diagram of one of the dimers of the TpCS−OAA complex (A and B subunits) is shown in Figure 5. The enzyme is a homodimer with each subunit having both a large and a small domain. Both the OAA and AcCoA binding sites are composed of residues from the large domain of one subunit and the small domain of the other. Catalytic residues arise solely from the large domains. Each TpCS subunit contains four W residues. W17, W115, and W348 are located in the large domain while W245 is located in the small domain.[5,6] The W residues and OAA are space-filled and colored by solvent exposure.

Changes in direct interactions such as van der Waals contacts or direct hydrogen bonding between substrates and W residues are not responsible for the fluorescence changes accompanying the formation of the various substrate and intermediate complexes of TpCS. Using the structures of TpCS−OAA[6] or TpCS−OAA−CMCoA (*62*) [or analogous PfCS−CitCoA (*63*)] complexes for distance calculations, no part of substrate molecules (Cit, CoA, or OAA) lies within 10 Å of W17, W115, or W245. The closest W348 atom is about 6.5 Å from OAA (or probably Cit) in the X-ray structure used here.

The emission maxima of all four W residues are quite blue [close to 315 nm (Figure 2)] as they are substantially buried. Figure 5 also shows spaced-filled versions of W residues and OAA colored by solvent accessibility with solvent exposure decreasing from red to deep blue. All four W residues are relatively solvent inaccessible with W17 having the greatest solvent exposure and W348 being completely buried. The emission maximum of the binary OAA complex remains unchanged, reflecting the structural information[6] that no major changes in solvent exposure of W residues have occurred. A more quantitative estimate is elaborated below.

Changes in Solvent Exposure of W348 on Formation of the OAA Binary Complex Are Unlikely To Be a Cause of W348 Quenching but May Contribute to the Enhancement Observed in Other W Residues. The lower panel of Figure 6 records the solvent accessibility of the indole ring of W residues for both the open form of the enzyme (no ligands present) and the four subunits of the OAA binary complex structure. The quantitative accessibilities were calculated using the program NACCESS with a probe 1.4 Å in diameter. Each of the four subunits in the asymmetric unit (two dimers) of the TpCS−OAA complex structure shows a slightly different conformation.[6] The rearrangement of the peptide backbone associated with the rotation of the small domain of one subunit with respect to the large subunit of the other has progressed to the greatest extent in the B and D subunits. Solvent accessibility of OAA is greatest in subunit D and least in subunit B. Even at the detail of hydrogen-bonding interactions within the active sites between OAA and universally conserved residues, there are significant differences. While there is no doubt that the OAA binary complex structure is predominantly closed, the changes that have been associated with the "closed" state of ternary complexes are not progressing in lock step in the binary complex (Kurz et al., unpublished observations of the TpCS−OAA−CMCoA complex X-ray structure and ref *62*). In some of the OAA binary complex subunits, the indole ring of the W residues 17, 115, and 245 shows increased solvent accessibility compared to either subunit of the unliganded, "open" form, and this may contribute to the enhanced fluorescence that these residues experience upon complex formation. Solvent accessibility of W348 remains zero in all complexes. The apparent heterogeneity of water content in the active sites of the four subunits of the X-ray structure of the complex is a complicating factor in the theoretical calculations (vide infra).

Other aspects of the global conformation change included in "closure" are not responsible for quenching W348 as is illustrated by the emission spectrum of the CitCoA complex (unquestionably a tightly closed form) whose fluorescence is enhanced significantly compared to the free enzyme and

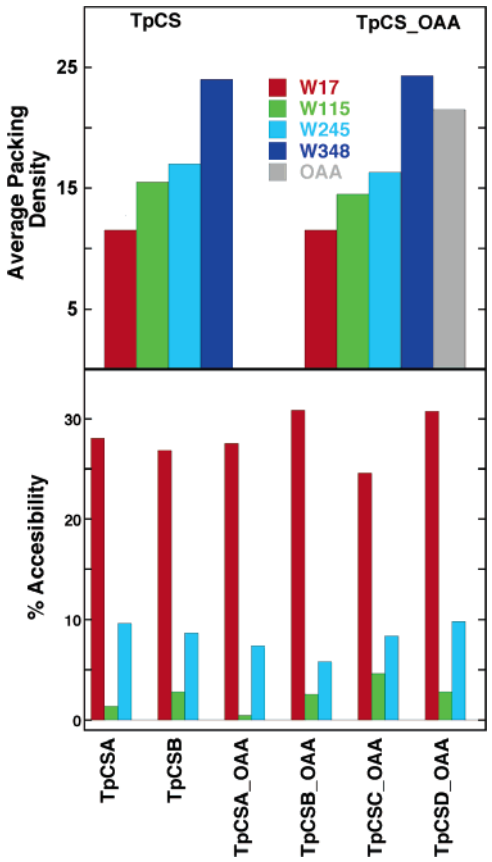

FIGURE 6: Upper panel: Packing density around W residues and OAA (defined as the number of residues within 6 Å of the residue and averaged over all subunits). Lower Panel: Solvent accessibility of the indole ring of each W residue to a 1.4 Å spherical probe (percent accessibility is defined as the ratio of the area actually accessible to the probe in the protein to that which would be accessible to the probe in free solution with the residue in the same conformation as found in the protein). Key: W17, red; W115, green; W245, turquoise; W348, blue; OAA, gray.

retains the vibrational shoulder apparent in the free enzyme (Figure 2). Note that CitCoA of course lacks the carbonyl of OAA. The binary complex with citrate, which also lacks the carbonyl of OAA, is also slightly enhanced compared to the free enzyme (Figure 2).[7]

The pronounced shoulder to the red of the W348 fluorescence maximum is due to unresolved vibrational structure and is frequently observed for tryptophans in closely packed, hydrophobic pockets that also contain some polar interactions (*64*). The upper panel of Figure 6 shows the packing density

[7] The two other ternary complexes studied, OAA−dethiaAcCoA and CoA−citrate, initially are somewhat puzzling. The slight partial quenching of the CoA−citrate complex may reflect the internal equilibrium of the enzyme and the presence of OAA−AcCoA in that equilibrium. Our kinetic studies suggest that the overall enzyme-bound reaction is more reversible than that in free solution; the partition ratio observed in Table 2 sets only a lower limit on reversibility (*7*). If the quenching observed in the product complex of TM is attributable to the presence of a small amount of a quenched OAA ternary complex, then it would represent about 20% of the ternary complexes, a quite plausible number. It may be possible to address this question in future experiments using time-resolved fluorescence spectroscopy as improved quantitation of our instrument is realized. The other puzzling question is why the dethiaAcCoA complex is not quenched if OAA has not reacted in that complex. The NMR experiments previously reported were interpreted to indicate (*8*) a lack condensation of OAA with dethiaAcCoA, but this conclusion may have been confounded by an intermediate exchange regime and may have to be reexamined.

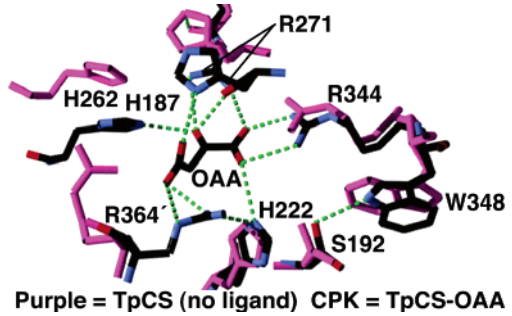

FIGURE 7: Superposition of unliganded and binary OAA complex structures featuring structural changes in the environment of W348. The unliganded enzyme is in purple. The OAA complex is in CPK representation. Note that different W348 rotamers are present in the complex and unliganded enzymes. [The rotamer change at this residue is found in other CS closed forms whether or not they possess a W residue at this position (*3*, *16*, *19*, *33*, *63*, *67*, *68*).]

surrounding each W residue and OAA. W348 is virtually wedged in place by its neighbors as reflected in its high packing density in comparison to that of other W residues.

The steric rigidity imposed by its environment may also account for the nearly monoexponential decay of W348 fluorescence (vide infra). The multiexponential decay of tryptophan or simple tryptophan amides in solution is thought to arise from heterogeneous conformations and solvent interactions (*65*, *66*) that are not present in the rigid and homogeneous protein environment of W348. These complexities aside, it is clear that the global conformation change accompanying OAA binary complex formation is not responsible for OAA quenching.

Experimental Probes Show That Local Structural Changes Are Not the Source of W348 Quenching in the OAA Binary Complex. Figure 7 shows the local structural features in the vicinity of W348 that differ between the unliganded enzyme and its OAA binary complex.

Although there were no acidic residues near W348 that are usually associated with a proton transfer quenching mechanism (Y, K, $-NH_4^+$), we studied the dependence of the quantum yield of TM and TM−OAA in D_2O buffers (Table 3) in order to examine this possibility. A substantial solvent isotope effect on the quantum yield (*42*) has been demonstrated when excited-state proton transfer is a major quenching mechanism. As shown in Table 3, no significant solvent isotope effects on the quantum yield of W348 in either TM or TM−OAA are observed; the small effects are probably indirect electrostatic ones arising from changes in the dielectric constant as a consequence of the presence of deuterium on the side chains of the solvent-exchangeable sites.

We have prepared a number of single site mutations to examine the effects of several of the residues shown in Figure 7 to the quenching observed in the OAA complex. Because these mutants were prepared using the WT template, their relative quantum yields on OAA complex formation should be compared to the quenching observed for WT−OAA rather than that for TM−OAA.

The new hydrogen bond between the indole ring and the side chain of S192 does not play a role in the quenching of the OAA complex. Recent studies (*47*, *48*) suggest that the presence of a S192 alcoholic oxygen H-bonded to the ring HN could contribute to the quenching by amides directly linked to W348 because of electrostatic stabilization of the resulting CT state. To clarify this issue, we prepared S192A and found it to be stable and active with the same p*I* as WT (Figure 1). We found somewhat greater quenching by that mutant on formation of the S192A−OAA complex than in the WT (Table 3).

The presence of the R344 residue and its reorientation when OAA binds are not the major factors in the W348 quenching observed in OAA binary complexes, but its charge likely plays a role. We prepared and studied two substitutions for this residue, R344K and R344M.[4] Despite considerable perturbations (vide infra) observed in the R344M mutant, the intrinsic fluorescence of W348 is substantially quenched in both R344M and R344K binary OAA complexes.

The R344K mutant is produced in good yield; it is stable and active, but it binds OAA with diminished affinity at pH 8.00 (Table 3). The shapes of the emission spectra of both the free and OAA complexes of R344K were nearly identical to that of WT. While considerable quenching is observed in the R344K−OAA complex (at pH 7 it is the same as WT at pH 8; Table 3), the presence of more unprotonated K344 (as compared to R344 at the same pH) is almost certainly responsible for the slightly diminished quenching. Anticipating our later discussion (vide infra), our theoretical calculations have repeatedly underscored the need for a large, positive potential difference between the indole ring and the OAA. K is shorter than R, and its charge is less delocalized. The observation of slightly less quenching by R344K at the same pH when compared to WT is in accord with our understanding of OAA itself as the primary electron acceptor as discussed below. Furthermore, the theoretical calculations clearly demonstrate that the reorientation of R344 that occurs as it rotates to hydrogen bond to OAA does not in itself contribute to the quenching in the OAA complex.

The R344M protein is obtained in very low yield and is difficult to purify; its activity is low and unstable. However, as with all of the proteins in this report it migrates as a single band in both native p*I* and SDS−PAGE gels. Relative to WT, the emission spectrum of R344M is red shifted 4−5 nm with a maximum at 320 nm, and it lacks the characteristic shoulder of partially resolved vibrational structure characteristic of W348 in other TpCS mutants. Nevertheless, the binding of OAA significantly quenches the emission of R344M. The OAA affinity is so poor that the titration curve remained nearly linear at the highest concentration of OAA studied (10 mM) so that we cannot extrapolate to obtain a spectrum of the fully formed complex. While the electrostatic environment of W348 is profoundly perturbed in R344M, the presence of OAA in the active site still quenches its emission.

Thus, we are led to the conclusion that the presence of OAA within the active site is the key feature underlying the quenching of W348 emission.

Bimolecular Quenching of W Fluorescence by Trimethylpyruvate, an OAA Model. Early results from molecular dynamics calculations also suggested that the presence of OAA within the active site was itself responsible for the strong quenching of W348 that accompanies complex formation. To further understand the role of OAA in the quenching of W348 in the complex, we have undertaken dynamic quenching solution experiments using the W analogue *N*-acetyl-L-tryptophanamide (NATA). The high

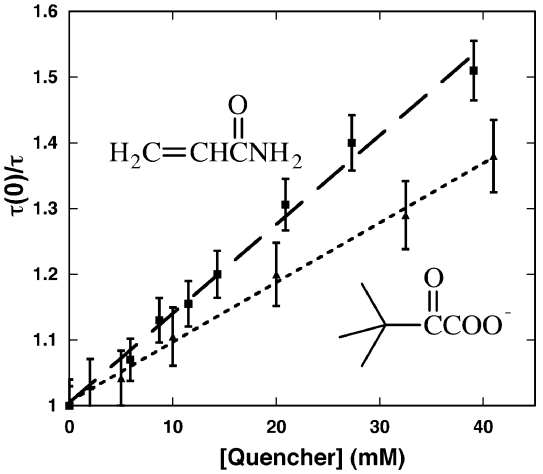

FIGURE 8: Stern−Volmer plots for the quenching of NATA by acrylamide (boxes, upper data set) and TMP (triangles, lower data set) in 50 mM EPPS buffer and 0.1 mM EDTA, pH 8, at 20 °C. Also shown are the linear regression results (dashed lines). Error bars were determined from the support plane errors for the NATA lifetimes (68% confidence level) by quadrature.

optical densities of millimolar solutions of OAA in the near-UV (due to the presence of the enol form)[3] preclude its use as a model quencher. Using TMP, which can exist in only the keto form, substantially reduced the inner filter effect. All α-keto acids (including TMP) still have a moderate absorption that is high enough to make lifetime experiments preferable over steady-state experiments to avoid an inner filter correction altogether. The limited solubility of TMP in aqueous buffers (50 mM) also limits the concentration range of quenching experiments. Stern−Volmer plots of TMP quenching of NATA fluorescence are shown in Figure 8.

To test the ability of our instrument to accurately determine bimolecular quenching constants from the lifetime changes expected at such low concentrations of quencher, experiments were carried out under identical conditions using well-studied acrylamide as the quencher. These results are also shown in Figure 8. Over the range 0−40 mM, positive deviations from Stern−Volmer behavior in this system are not expected (*56*). The decay of NATA was adequately fit to two exponentials; 80−90% of the amplitude was contained in a 2.79 ns component, which agrees well with the reported single exponential decay value of 2.87 ns (*69*). Using eq 3, the bimolecular quenching constant for acrylamide is found to be 5.1×10^9 M^{-1} s^{-1} at 20 °C, in good agreement with the literature value (*70*) of 5.9×10^9 M^{-1} s^{-1}. As seen clearly in the Stern−Volmer plots, the OAA analogue TMP has moderate quenching ability with a bimolecular quenching constant of 3.2×10^9 M^{-1} s^{-1}, approximately 60% that of acrylamide. Thus, the quenching of W348 by the presence of OAA in the active site is an entirely reasonable proposition.

Quantitative Estimates of W Fluorescence in TpCS and Its Complexes. Panels A−C of Figure 9 display the ground → lowest CT and ground → ^1L_a computed vertical transition energies during 20 ps dynamics trajectories for W17 (Figure 9A), W348 (Figure 9B), and the W348−OAA (Figure 9C) supermolecule, respectively. In each of these simulations, the protein was the A chain of the crystal structure.

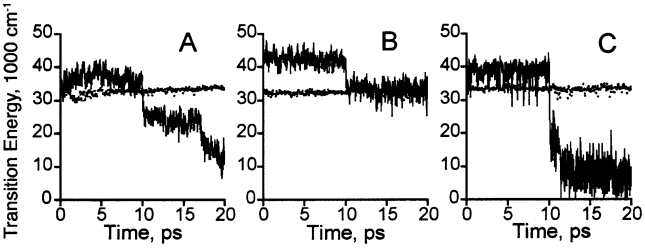

FIGURE 9: Representative QM-MM trajectories showing ^1L_a (points) and lowest local amide CT (line) transition energies. During the first 10 ps the electron density is that of ^1L_a, and from 10 to 20 ps it is that for the CT state. Panels: (A) W17; (B) W348 in TpCS−OAA; (C) W348−OAA supermolecule in TpCS−OAA with H187 protonated. In (C), the lowest CT state often has OAA as the electron acceptor during the first 10 ps, although sometimes it is one of the W348 amides. OAA is the acceptor at all times after 10 ps.

For the W17 (Figure 9A) and W348 (Figure 9B) trajectories, H187 is neutral, but for the W348−OAA supermolecule (Figure 9C, W348−OAA H187+ in Table 5), H187 is protonated. The geometry used for these trajectories is that of the CT state. The energies are relative to the ground electronic state also in the CT geometry. During the first 10 ps the W charge distribution is that of the fluorescing ^1L_a state, but during the last 10 ps the distribution is that for the lowest CT state for which an electron has been transferred from the indole ring to one of the two backbone amide groups on the W (Figure 9A,B) or to one of the two amides or to the OAA (Figure 9C). The last part of the trajectories always shows relaxation of the CT energy due to solvent and side chain response to the considerably different charge distribution in the CT state. Quenching occurs if this relaxation brings the poorly emitting CT state irreversibly below the ^1L_a state.

Table 5 shows the quantum yields predicted from trajectories of the type shown in Figure 9 using the same procedure that was successfully applied to W quantum yields for 24 Trps in 17 proteins (*48*). In this procedure, the average electron transfer rate increases as the average CT−^1L_a energy gap decreases and as the fluctuation amplitude of the gap (standard deviation) increases. As can be seen from Figure 9A, the small gap and large fluctuations predict a very low quantum yield (0.024) for W17 compared to about 0.3−0.35, the maximum values typically seen for W in proteins. The predicted quantum yields in Table 5 for W115 and W245 are also much lower than 0.3. These results agree with the experimental observations (Table 3 and Figure 3).

For W348, which dominates the observed fluorescence, as inferred from the observed quantum yield of 0.27 for the TM mutant, the predicted quantum yield was found to be sensitive to the presence of a single water molecule in the model. In the first trajectory we performed that monitored electron transfer quenching of W348, labeled W348(1) in Table 5, one of the 6867 waters added by the solvating process was placed in a cavity near the carbonyl of G347. This water occasionally H-bonded to the G347 carbonyl oxygen, thereby greatly stabilizing the CT state arising from electron transfer from the W348 ring to the G347 amide. Primarily because of this, the predicted quantum yield from W348 was low (0.10). However, a similar trajectory, labeled W348(2), starting with the same coordinates except with the single nearby water deleted, predicted negligible ET quench-

Table 5: Computed Energy Differences, Standard Deviations, Electron Transfer Rates, and Quantum Yields

name	structure	CT−^1L_a gap ($cm^{-1} \times 10^3$)	SD ($cm^{-1} \times 10^3$)	ET rate constant ($\times 10^7\ s^{-1}$)	predicted quantum yield[a]
W17	TpCS (no ligand)	4.45	2.45	260	0.024[b]
W115	TpCS (no ligand)	7.70	2.37	21.3	0.16[b]
W245	TpCS (no ligand)	6.23	2.15	57.4	0.1[b]
W348 (1)	TpCS (no ligand)	6.13	2.18	64.7	0.1[c]
W348 (2)	TpCS (no ligand)	10.13	2.29	1.15	0.37[c]
W348	TpCS−OAA	10.08	1.83	0.16	0.38[c]
W348−OAA	TpCS−OAA	9.31	1.64	0.23	0.38[c]
W348−OAA H187+	TpCS−OAA	5.22	2.39	157.0	0.05[c]

[a] Using parameters optimized for amide quenching (*48*). [b] Using fluorescence and radiative lifetimes for 3-methylindole in tetrahydrofuran (*45*). [c] Using fluorescence and radiative lifetimes for 3-methylindole in cyclohexane (*45*).

ing, which is consistent with experiment. By inference, there is probably no water present in the G347 cavity, although this is the type of phenomenon that could explain the 0.68 ns minor component in the fluorescence decay of TM (Table 4). However, the issue will remain equivocal until a structure of the apoenzyme is obtained with a sufficient resolution to include waters.

It is worth noting at this point based on the crystal structure of the OAA complex that it is very unlikely that OAA binding brings in a water near W348 that could hydrogen bond to one of the local amides allowing fast ET to the hydrated amide (as in one of the simulations of the unliganded enzyme). Although a water molecule was brought in near G347 when solvating the unliganded enzyme, this never happened with the OAA complex. There is no gap in the structure of the complex as there is in the unliganded enzyme.

High W348 quantum yields were also predicted using the TpCS−OAA structure (lines 6 and 7 of Table 5), which contains OAA and has W348 in a different rotameric conformation than that in the free enzyme (seen in Figure 7). In the first of these, only local amide quenching was monitored, although the electrostatic effect of the OAA on this quenching was included. Independent analysis of the contribution of individual amino acid residues to the electrostatic perturbation of the local amide CT state energies confirms that neither the OAA dianion nor R344 movements upon binding of OAA are significant enough to be the cause of the quenching upon OAA binding.

In the second TpCS−OAA trajectory, labeled W348−OAA (line 7 of Table 5), the QM part was a W348−OAA supermolecule, and quenching by the OAA was monitored in addition to the local amide quenching. In this trajectory (shown in Figure 9B), the indole → OAA CT state energy was always about 1 eV above that for electron transfer to the C-terminal amide of W348. This result is not in agreement with the strong quenching observed for W348 when OAA is bound. However, we note that were the QM calculation performed in a vacuum, the lowest CT state involving transfer to the doubly negative OAA from indole is about 5 eV above the amide CT state, because of the −2 charge; the (simulated) environment provided by the protein has lowered the CT state by 4 eV.

One reason for this discrepancy could be that we used only a monomer protein chain in the simulations, whereas the dimer is the form in solution displaying the quenching. For the dimer, R364 of one chain is H-bonded to the terminal carboxylate of the OAA in the other chain. The extra positive charge from this R364 and its neighbor, R361, could greatly stabilize the OAA CT state, leading to a prediction of strong quenching. We ran two simulations to test this: one in which residues 359−381 of the B crystal structure subunit were included with the A subunit and one in which residues 359−381 of A were included with the B subunit. Similar results were obtained from these two simulations, both again predicting a high quantum yield (∼0.25), despite stabilization of the OAA CT state by ∼2 eV by the opposite chain arginines. The reason is that in these simulations the opposite chain fragment arginines polarize the water to create a large destabilizing contribution that effectively cancels the direct effect of R364, R361, and R366. Perhaps this is an artifact of not including the entire dimer in the simulation, but simulating the dimer is beyond our means at this point.

Two other possible reasons for the discrepancy are presented next. Because of the −2 charge on the OAA, a reasonable hypothesis is that a proton is carried into the protein when OAA binds, despite the three arginine residues near the bound OAA. To test this, a trajectory was carried out with H187 protonated. H187 lies near OAA, and the increased positive potential near the OAA should greatly stabilize the OAA CT state. Figure 9C shows this trajectory, for which the smaller ^1L_a−CT gap leads to a prediction of strong quenching by the OAA. In this case, addition of the positive charge once again causes a decrease of about 1 eV in stabilization by water, but this does not cancel the nearly 3 eV of increased stabilization by the protonated H187.

A second hypothesis is that OAA quenches through Förster resonance energy transfer (FRET). This mechanism must be considered even though the molar absorptivity of OAA is only 30 $M^{-1}\ cm^{-1}$ [estimated from the absorption spectra of trimethylpyruvate and dimethyl-OAA (*71*)], because its absorption band strongly overlaps the fluorescence emission spectrum of W348, and its carbonyl carbon lies only about 10 Å away from the center of the indole ring. The absorption spectrum of TMP and the fluorescence spectrum, lifetime, and quantum yield of W348 in TM give a *maximum* Förster transfer rate of $5 \times 10^8\ s^{-1}$, assuming perfect projection of side-by-side transition dipoles. Although this rate would reduce the quantum yield to about 0.08, it would give a lifetime of 1.4 ns if the system were homogeneous. However, from Figure 4 and Table 4 we see that 78% of the observed fluorescence decays with a rate of $1 \times 10^{10}\ s^{-1}$, i.e., 50 times faster, an impossibly high rate for FRET quenching unless the W−OAA distance was nearly 5 Å shorter than given by the X-ray structure. This is an extremely conservative conclusion. In the Supporting Information we give reasons

for expecting the maximum transfer rate to be an order of magnitude smaller yet. The OAA absorbance is from an n−π* transition associated with the carbonyl bond and is dipole forbidden when planar. In formaldehyde it gains intensity primarily through vibronic coupling from the umbrella mode involving pyramidalization about the carbonyl carbon and induces a transition dipole directed in-plane and perpendicular to the C═O bond. This part of the absorptivity has a $\kappa^2 \approx 0$ in the crystal because that direction is essentially perpendicular to the W348 transition dipole (which lies in the indole ring plane and pointing roughly between N1 and C4). The remaining intensity (∼12%) comes from the asymmetric CH stretch, which induces intensity polarized perpendicular to the plane, a direction that is nearly parallel and side by side with the W348 moment; i.e., this part has $\kappa^2 \sim 1$. Thus, we expect that the total κ^2 is ∼0.12, which is much too small to account for the observed quenching.

The conclusion that electron transfer is the primary quenching mechanism is strongly reinforced by recent data with 5-FW-labeled TpCS, for which the OAA-induced quenching is almost half that for the unlabeled case (see Supporting Information for actual spectra). Broos et al. (*72*) have demonstrated that 5-F substitution most likely strongly diminishes electron transfer from excited W. Accurate calculations of the ionization potential (IP) of 5F-3-methylindole relative to 3-methylindole show that electron transfer must be considerably reduced for 5F-W (T. Liu and P. R. Callis, unpublished results). On the other hand, the 7 nm red shift of fluorescence from 5F-W is predicted to reduce the FRET rate by only about 5%.

What Can We Resolve at This Point? Thus, while Förster transfer may account for a small part of the quenching, electron transfer, most likely to the OAA, seems to be necessary to account for the fast (0.1 ns) quenching observed. That we can be decisive on this point is because the Förster transfer can be comfortably eliminated. Given the uncertainties in our relatively untested theoretical methods, uncertainties in the protein structure, and experimental challenges, we are forced to be more cautious regarding the question of whether the electron transfer is to OAA and especially whether this requires an unexpected additional proton near the OAA, as the theory in its present form claims. Below we survey the reasons for our cautiousness.

What Are the Possible Deficiencies in Our Calculations? The calculations of Figure 9 and Table 5 suggest that another proton, either on the OAA itself or on one of the nearby histidines, is required to make the electron transfer energetically favorable to the OAA dianion. This result has driven several new simulations and experiments, but the complexities of predicting electrostatic energies have left a high degree of ambiguity.

It is appropriate to keep some perspective. It is remarkable that our calculations have gone most of the way in explaining the experimental results. It is very difficult to transfer an electron from the excited Trp side chain to a −2 ion. In a vacuum, the lowest CT state is with OAA giving the electron to W, at 2.5 eV below the ^1L_a state. The lowest CT for transfer from excited W to OAA is 8.5 eV above ^1L_a. This active site is the hottest spot for which we have done simulations to date. Using an abbreviated model that only includes part of the dimer, the protein environment stabilizes the CT to OAA by about 4 eV. If it did so by just 1 more eV, massive quenching would be predicted.

First We Examine Some of the Necessary Assumptions Inherent to the Method That Might Be in Error. The MM might not adequately stabilize the OAA^{-3} radical. We scale the QM charges down by 0.80 because that created the correct wavelength shift for 3-methylindole in water (*46*). Or, the polarization of the water may be exaggerated, despite the scaling. If the water polarization contributed 1 eV less, there would be agreement. The method, however, does perform well for the relative quenching by histidine compared to histidine cation (T. Liu and P. R. Callis, manuscript in preparation). Perhaps the QM is not predicting a low enough CT state energy. We are subtracting 4000 cm^{-1}, which worked well for the amides (*48*) but maybe this is not enough: the physical significance of this parameter is not yet established because it may be compensating for treating the interaction element as an empirical constant. Unlike the Förster transfer interaction, the electron transfer interaction element is much less certain because it depends on the overlap of the donor and acceptor wave functions, which can be extremely sensitive to orientation because of their nodes. Generic estimates of maximum electron transfer rates are on the order of 1×10^{11} s^{-1} using the common formula (*73*) rate constant $= 10^{13} \exp(-\beta(R - 3))$, with β having a value of 1.0−1.4 $Å^{-1}$, and R is the closest donor−acceptor atom−atom distance (∼6 Å). Perhaps the interaction is much larger than the global 10 cm^{-1} that was deduced for quenching by amide systems. This cannot be completely ruled out, because 10 cm^{-1} is rather small for the typical indole−amide distances found in proteins. It might be small because of an unfavorable orbital overlap for amides but could be more favorable for the indole OAA interaction in TpCS. However, the coupling would have to be 20 times higher (rate constant 400 times higher) for the indole−OAA using the current energy parameters, which seems improbable. We also use the amide Franck−Condon factors here, but these are dominated by the lengthening of the C═O bond, as is expected also for OAA.

The most promising deficiency (and one that can eventually be remedied) is our present inability to include the entire dimer in the calculations. The considerably delocalized source of the positive potential of the TpCS active site is underscored by a CAST analysis (*74*). The active sites are deep pockets with a volume of 350 $Å^3$ (averaged over the four subunits in the unit cell). The pockets are lined with positive residues from both subunits of the dimer. For the active site whose catalytic residues originate in the large domain of subunit B, the active site pocket is lined with positively charged side chain atoms from the obligatorily positive residues R256(B), R263(B), R271(B), R344(B), R361(A), and R364(A) as well as the potentially positive atoms from H187(B), H262(B), and H222(B). The sole negatively charged residue is the active site base, D317(B). The mouth of the same pocket (with an area of 32 $Å^2$ and length of 42 Å) has positively charged atoms from R256(B), R263(B), and R361(A). The accurate calculation of the positive potential at OAA is a difficult problem.

It is worth noting that some ternary complexes of TpCS−OAA, most notably the OAA−CoA and OAA−CMCoA complexes, show about the same strong quenching as observed in the binary complex used for the present

calculations. In these complexes [TpCS−CMCoA−OAA structure (*62*)], the CoA molecule forms a U-shaped plug that displaces most of the water from the active site and renders it solvent inaccessible. This same burial of the active site occurs in other citrate synthase ternary complexes (*16*, *63*, *67*, *75*) including the CoA−citrate product complex and is believed to be an essential part of the enzymes' catalytic strategy. In the product complex, strong quenching is not observed (Figure 2) because most of the OAA is now present as citrate.[7]

Even if we include the entire dimer, we are not absolutely certain of the appropriate geometry for the calculations. There is asymmetry in the X-ray structure of the OAA binary complex.[6] Each active site in the four subunits (two dimers) in the unit cell has slightly different numbers of resolved water molecules, different degrees of bulk solvent accessibility (Figure 6), and changes in the orientation of some side chains, including R364 from the other subunit. Prospects for obtaining a higher resolution X-ray structure of TpCS−OAA are good and may clarify this issue. More certainty in the structure data will further justify future calculations that include the entire dimer. Using the structure of a quenched ternary complex in these calculations might also be revealing as these are much more symmetrical [TpCS−CMCoA−OAA structure (*62*)].

If Additional Positive Electrostatic Potential Is Needed, What Is Its Source? Are Any of the H Residues in the Active Site Charged? Do Any Take Up a Proton When OAA Binds? Is OAA Itself Bound as the Monoanion? While we believe it is possible, even likely, that the need for more positive potential will disappear with more sophisticated calculation and higher resolution structural data, we have investigated each of these possible sources of positive electrostatic potential in the neighborhood of OAA.

At present, we can be reasonably certain that the extra proton is not present in the unliganded protein. It is more difficult to rule out the uptake of a proton upon OAA binding; several experiments are qualitatively consistent with such an uptake, but the effects are too small to be definitive. We first examine whether one of the three active site histidines is protonated. (The protonation state of the histidines is of considerable interest to mechanistic enzymologists.[8]) If one of these imidazole side chains has a high pK_a so that it is positively charged (under conditions where we observe quenching of W348), then we would expect consequences when we mutate H to Q since Q has an obligatorily neutral side chain. We constructed the three active site mutants in which each of the three H residues had been changed to Q and studied their properties.

One probable consequence is that OAA binding should be substantially weaker in the presence of a reduced positive electrostatic potential. While the affinity of OAA is modestly reduced for the two mutants H262Q and H222Q, it is very weak (K_D ~600 μM, Table 3) for H187Q. This result is consistent with the hypothesized protonated H187 used in the theoretical calculations.

In addition, if a positively charged H side chain is essential to efficient electron transfer to OAA and to W348 quenching, then we would expect substantially less quenching when that side chain is replaced with Q. Fluorescence in H262Q−OAA is quenched about the same extent as in WT, and in H222Q−OAA it is quenched somewhat more (Table 3).

Because of its very high K_D for OAA, determination of the relative quantum yield for H187Q−OAA required the use of front face fluorescence to maximize the signal and allow determination of the substantial inner filter correction (about a factor of 4). The results at 10 mM OAA (about 10 times K_D) are reported in Table 3 along with WT under the exact same conditions. See the Supporting Information for the actual spectra used for these calculations. There is modestly less quenching in H187Q than in WT (relative QY of 0.62 vs 0.44). While this result seems consistent with a contribution to the quenching from a protonated H187, two other observations suggest caution. First, there is greater quenching in H222Q (0.37) than in WT. Second, the formation of the ternary complex with CMCoA further reduced the fluorescence of H187Q (relative QY = 0.58 vs 0.62) while the same ternary complex of WT has increased fluorescence (relative QY of 0.54 vs 0.44). An examination of the series of single W mutants attributes this increase to W115 in WT (data not shown). Also note (Table 2) that the kinetic constants for H187Q suggest that it is close to a pure binding mutant (H187Q binds ground states and transition states equally). K_D and K_M values are elevated. On the other hand, the values of the overall k_{cat}, the partitioning of the CitCoA intermediate, and even the extent to which the hydrolysis step is faster than condensation are indistinguishable from those of wild type. If the protonation of H187 is important to the ability of the OAA carbonyl to accept an electron or react with the AcCoA carbanion, it is entirely possible that some compensatory change has occurred in H187Q, but we view this as unlikely.

Furthermore, if the pK_a of the histidine is elevated and comparable to that of the usual basic residues (such as K) as suggested by the QM-MM calculations, then the mutation to Q will remove a positive charge and lower the p*I* of the protein. In confirmation of this reasoning, Figure 1C shows that deletion of a single positively charged residue as in R344M results in an easily detected change in p*I*. In contrast, Figure 1B shows that all active site H to Q mutants have the same p*I* as WT.[9,10] So at least in the unliganded enzyme it seems that none of the H residues is protonated.

Considering now the uptake upon binding OAA possibility, we first consider whether one of the active site H residues might be taking up a proton when the OAA complex forms. If so, we would expect that the pH dependence of OAA affinity would be altered in that mutant, but the pH dependence of OAA affinity for WT, H222Q, and H262Q

[8] The protonation state of the active site histidines is at the center of a novel and controversial proposal to account for several enzymes' extraordinary ability to produce and stabilize a reactive carbanion intermediate (*9*−*11*). Knowles et al. (*12*−*14*) first proposed that the neutral imidazole side chain could act as a general acid in this role. While a protonated imidazole would also certainly stabilize the carbanion, the Knowles calculations indicated that the enolate would be overstabilized, creating a thermodynamic pit incompatible with efficient catalysis. The Knowles proposal would require a histidine with an unusually low first pK_a if it remains neutral over the studied pH range and a low second pK_a to act as a general acid to facilitate enolate protonation. This is contrary to what seems to be required by the QM-MM calculations since what they require is a histidine with a high first pK_a. Theoretical calculations from Kollman's group (*15*) seem to obviate the necessity of a neutral imidazole general acid and support the existence of an enolate intermediate stabilized by simple hydrogen bonding to H222, although they also suggest that an additional positive charge in the system would be advantageous.

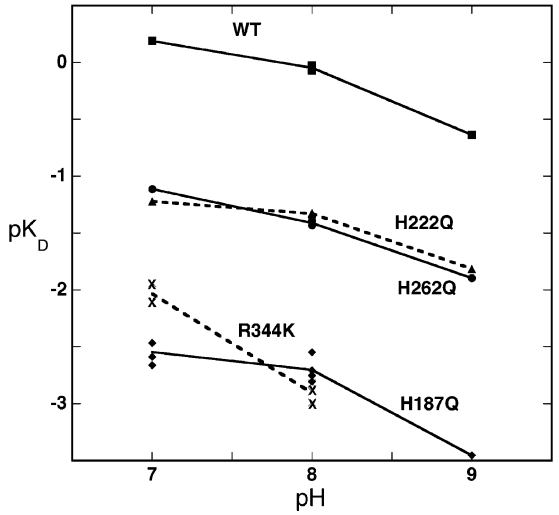

FIGURE 10: Dependence of OAA pK_D on pH for WT, active site H to Q mutants, and R344K (pK_D values were calculated from K_D values in micromolar). Key: WT, filled boxes connected by a solid line; H222Q, filled triangles connected by a dotted line; H262Q, filled circles connected by a solid line; R344K, X's connected by a dashed line; H187Q, filled circles connected by a solid line.

are very similar. The data for H187Q suggest that there may be slightly more pH dependence of OAA affinity for that mutant. The uncertainty is large.

The pH dependence of pK_D data for R344K is similar to that for H187Q but is shifted by about 1 pH unit. The p*I* experiments (Figure 1C) indicate that K344 is neutral in the free enzyme as R344K has the same p*I* as R344M. The pH dependence for this mutant is considerably steeper than that for the H to Q mutants as shown in Figure 10, the R344K affinity for OAA increasing about 5-fold between pH 7 and pH 8. About twice this dependence of K_D on pH was reported for the binding of the carboxylic enolate analogue inhibitor, CMCoA (*27*), which is known to take up a proton on ternary complex formation from NMR (*76*) and X-ray structure data (*67*). Suggestively, the quantum yield of R344K is also less than that of the WT at the same pH (Table 3). Only at pH 7 does R344K show as much quenching as does WT at pH 8.0. While less extensive kinetic studies of R344K have been done in comparison to H187Q, this mutant (Table 2) also appears close to a pure binding mutant since its k_{cat} is slightly greater than that of WT.

[9] The p*I* for TpCS calculated from the amino acid composition is 7.7, and this value is confirmed under denaturing conditions (*7*). Since the p*I* of 8.9 for the native protein is quite high (ref *7* and Figure 1A,B), one or more residues has a pK_a outside the usual range. TpCS has a total of 44 strongly acidic residues that we expect to be negatively charged (19 D and 25 E residues) and an equal number (44) of basic residues that we expect to be positively charged (17 R and 27 K residues). The remaining potentially ionizable groups are the 6 H residues and 20 Y residues. In addition to the three active site H to Q mutants, we have also constructed single mutants of the three H residues outside the active site (H141N, H290Q, and H351Q) and found that the p*I* values of these proteins are also unaltered from that of WT (Kurz, unpublished data).

[10] It is difficult to extend the experiments to lower pH due to the increasing instability of OAA and difficult to extend the experiments to higher pH because of the weakened affinity for OAA. The weak binding at high pH requires high OAA concentrations to define the titration curve in turn necessitating large inner filter corrections at both the excitation and emission wavelength. We found these corrections very difficult to reproduce.

Finally, we consider whether one of the two OAA carboxylates becomes protonated upon binding to the enzyme? This would mean that the K_D for *bound* OAA be $\sim 10^4$ times smaller (i.e., 10^{-9} or p$K_D = 9$) for $HOAA^{-1}$ than for OAA^{-2}. If this were the case, the pH dependence of the apparent K_D in the pH range of 7−9 would be considerably larger than we observe (Figure 10). Furthermore, if quenching by OAA requires one of the carboxylates to be protonated, then the pH dependence of quenching in the OAA binary complex would be much steeper than that which we observe. We observe only a small increase in the quenching with lower pH (Table 3). Consistent with this proposal, however, is the observation that the C-13 chemical shifts of the carboxyl carbons of bound OAA do shift in the same direction. We do not consider this definitive, however, because the C-13 protonation shift is small and sensitive to environment.

If a proton is taken up when OAA binds, then the p*I* of the complex should reflect this change. Unlike the case of tight DNA−protein complexes, it is not possible to demonstrate a p*I* gel shift for TpCS−OAA because the affinity of OAA for the protein is not high enough to maintain the integrity of the complex against the electrostatic forces pulling it apart in the electrophoresis apparatus.

CONCLUSION

Changes in enzyme tryptophan fluorescence that accompany the binding (and turnover) of substrates, inhibitors, and effectors are potentially much more than simple physical probes of kinetic and equilibrium processes. Advances in theoretical understanding of tryptophan photophysics together with experimental results such as those reported here with TpCS show that it is possible to understand changes in protein tryptophan fluorescence in some detail and underscores the potential usefulness of these changes as mechanistic probes.

We have presented strong evidence that electron transfer is the mechanism for quenching W348 in the TpCS−OAA complex. Other mechanisms including Förster transfer, internal conversion, and excited-state proton transfer are excluded by theoretical and experimental arguments. We conclude the acceptor is OAA itself. The present theoretical simulations are able to provide 4 of the 5 eV needed to make the OAA carbonyl the preferred electron acceptor from the excited indole. The need for more stabilization is questioned mainly because of the inability to include the whole dimer in our present calculations, but uncertainties in some of the necessary parameters for the calculations might also be contributors. Nonetheless, proton uptake upon formation of the binary OAA complex (a protonated His or on OAA itself) as an additional source of electrostatic stabilization is considered in some detail. While some data in favor of this hypothesis are presented, a definitive conclusion is not yet possible. What is clear, however, is that the forces in the protein environment that make the OAA carbonyl the preferred electron acceptor from the W348 excited state are also the forces responsible for increasing carbonyl reactivity toward condensation with the AcCoA carbanion.

Future Work. Calculations including the entire dimer utilizing higher resolution X-ray structures will be performed when greater computation power and higher resolution

structures become available. The more symmetrical ternary complexes with their less solvent accessible active sites should prove more amenable to resolving the problems introduced into the calculations by water polarization. From the experimental perspective, it will be instructive to examine other Archaeal citrate synthases (PfCS and DsCS) differing in their structural details from TpCS but conserving a W at the equivalent position. We could engineer a W residue into the eukaryotic CS proteins that have a V at this position as further proof of principle.

In addition to the quenching in the OAA binary complex and in most ternary complexes containing OAA, large fluorescence enhancements occur upon equilibrium formation of the ternary complex with the partial substrate, dethiaAcCoA (*8*), and a large transient enhancing change is even noted during formation of the TpCS−OAA enolate analogue complex with CMCoA (L. C. Kurz, unpublished observations). We are working to obtain structures of these ternary enzyme complexes so that we may test the ability of theoretical calculations to explain these other interesting fluorescence changes.

SUPPORTING INFORMATION AVAILABLE

More detailed calculations further diminishing the possibility that FRET to OAA is responsible for the quenching of W348, experimental data on 5-FTrp-labeled TPCS that further support our conclusion that electron transfer is the primary quenching mechanism in the OAA−TpCS complex, and spectra that were used to calculate the relative quantum yields by front face fluorescence at high OAA concentrations for WT and H187Q and their OAA and OAA−CMCoA complexes. This material is available free of charge via the Internet at http://pubs.acs.org.

REFERENCES

1. Frieden, C., and Fernandez-Sousa, J. (1975) Kinetic studies on pig heart cytoplasmic malate dehydrogenase, *J. Biol. Chem. 250*, 2106−2113.
2. Gallivan, J. P., and Dougherty, D. A. (1999) Cation-pi interactions in structural biology, *Proc. Natl. Acad. Sci. U.S.A. 96*, 9459−9464.
3. Russell, R. J., Hough, D. W., Danson, M. J., and Taylor, G. L. (1994) The crystal structure of citrate synthase from the thermophilic archaeon, *Thermoplasma acidophilum*, *Structure 2*, 1157−1167.
4. Zhi, W., Srere, P. A., and Evans, C. T. (1991) Conformational stability of pig citrate synthase and some active-site mutants, *Biochemistry 30*, 9281−9286.
5. Kurz, L. C., Ackerman, J. J., and Drysdale, G. R. (1985) Evidence from ^{13}C NMR for polarization of the carbonyl of oxaloacetate in the active site of citrate synthase, *Biochemistry 24*, 452−457.
6. Guex, N., and Peitsch, M. C. (1997) SWISS-MODEL and the Swiss-Pdb Viewer: An environment for comparative prtoein modeling, *Electrophoresis 18*, 2714−2723.
7. Kurz, L. C., Drysdale, G., Riley, M., Tomar, M. A., Chen, J., Russell, R. J., and Danson, M. J. (2000) Kinetics and mechanism of the citrate synthase from the thermophilic archaeon *Thermoplasma acidophilum*, *Biochemistry 39*, 2283−2296.
8. Kurz, L. C., Roble, J. H., Nakra, T., Drysdale, G. R., Buzan, J. M., Schwartz, B., and Drueckhammer, D. G. (1997) Ability of single-site mutants of citrate synthase to catalyze proton transfer from the methyl group of dethiaacetyl-coenzyme A, a non-thioester substrate analog, *Biochemistry 36*, 3981−3990.
9. Bash, P. A., Field, M. J., Davenport, R. C., Petsko, G. A., Ringe, D., and Karplus, M. (1991) Computer simulation and analysis of the reaction pathway of triosephosphate isomerase, *Biochemistry 30*, 5826−5832.
10. Karplus, M., Evanseck, J. D., Joseph, D., Bash, P. A., and Field, M. J. (1992) Simulation analysis of trisoe phosphate isomerase: conformational transition and catalysis, *Faraday Discuss. 93*, 239−248.
11. Alagona, G., Ghio, C., and Kollman, P. A. (1995) Do enzymes stabilize transition states by electrostatic interactions or pK_a balance: the case of triose phosphate isomerase (TIM), *J. Am. Chem. Soc. 117*, 9855−9862.
12. Lodi, P. J., and Knowles, J. R. (1991) Neutral imidazole is the electrophile in the reaction catalyzed by triosephosphate isomerase: structural origins and catalytic implications, *Biochemistry 30*, 6948−6956.
13. Komives, E. A., Chang, L. C., Lolis, E., Tilton, R. F., Petsko, G. A., and Knowles, J. R. (1991) Electrophilic catalysis in triosephosphate isomerase: the role of histidine-95, *Biochemistry 30*, 3011−3019.
14. Lodi, P. J., and Knowles, J. R. (1993) Direct evidence for the exploitation of an alpha-helix in the catalytic mechanism of triosephosphate isomerase, *Biochemistry 32*, 4338−4343.
15. Donini, O., Darden, T., and Kollman, P. A. (2000) QM-FE calculations of aliphatic hydrogen abstraction in citrate synthase and in solution: reproduction of the effect of enzyme catlaysis and demonstration that an enolate rather than an enol is formed, *J. Am. Chem. Soc. 122*, 12270−12280.
16. Remington, S., Wiegand, G., and Huber, R. (1982) Crystallographic refinement and atomic models of two different forms of citrate synthase at 2.7 and 1.7 angstroms resolution, *J. Mol. Biol. 158*, 111−152.
17. Kurz, L. C., Nakra, T., Stein, R., Plungkhen, W., Riley, M., Hsu, F., and Drysdale, G. R. (1998) Effects of changes in three catalytic residues on the relative stabilities of some of the intermediates and transition states in the citrate synthase reaction, *Biochemistry 37*, 9724−9737.
18. Wiegand, G., and Remington, S. J. (1986) Citrate synthase: structure, control, and mechanism, *Annu. Rev. Biophys. Biophys. Chem. 15*, 97−117.
19. Liao, D. I., Karpusas, M., and Remington, S. J. (1991) Crystal structure of an open conformation of citrate synthase from chicken heart at 2.8-Å resolution, *Biochemistry 30*, 6031−6036.
20. Usher, K. C., Remington, S. J., Martin, D. P., and Drueckhammer, D. G. (1994) A very short hydrogen bond provides only moderate stabilization of an enzyme−inhibitor complex of citrate synthase, *Biochemistry 33*, 7753−7759.
21. Kurz, L. C., and Drysdale, G. R. (1987) Evidence from Fourier transform infrared spectroscopy for polarization of the carbonyl of oxaloacetate in the active site of citrate synthase, *Biochemistry 26*, 2623−2627.
22. Kurz, L. C., Drysdale, G. R., Riley, M. C., Evans, C. T., and Srere, P. A. (1992) Catalytic strategy of citrate synthase: effects of amino acid changes in the acetyl-CoA binding site on transition-state analog inhibitor complexes, *Biochemistry 31*, 7908−7914.
23. Gerlt, J. A., and Gassman, P. G. (1993) Understanding the rates of certain enzyme-catalyzed reactions: proton abstraction from carbon acids, acyl-transfer reactions, and displacement reactions of phosphodiesters, *Biochemistry 32*, 11943−11952.
24. Gerlt, J. A., and Gassman, P. G. (1993) An explanation for rapid enzyme-catalyzed proton abstraction from carbon acids: importance of late transition states in concerted mechanisms, *J. Am. Chem. Soc. 115*, 11552−11568.
25. Bayer, E., Bauer, B., and Eggerer, H. (1981) Evidence from inhibitor studies for conformational changes of citrate synthase, *Eur. J. Biochem. 120*, 155−160.
26. Remington, S. J. (1992) Structure and mechanism of citrate synthase, *Curr. Top. Cell Regul. 33*, 209−229.
27. Kurz, L. C., Shah, S., Crane, B. R., Donald, L. J., Duckworth, H. W., and Drysdale, G. R. (1992) Proton uptake accompanies formation of the ternary complex of citrate synthase, oxaloacetate, and the transition-state analog inhibitor, carboxymethyl-CoA. Evidence that a neutral enol is the activated form of acetyl-CoA in the citrate synthase reaction, *Biochemistry 31*, 7899−7907.
28. Arnott, M. A., Michael, R. A., Thompson, C. R., Hough, D. W., and Danson, M. J. (2000) Thermostability and thermoactivity of citrate synthases from the thermophilic and hyperthermophilic archaea, *Thermoplasma acidophilum* and *Pyrococcus furiosus*, *J. Mol. Biol. 304*, 657−668.
29. Russell, N. J. (2000) Toward a molecular understanding of cold activity of enzymes from psychrophiles, *Extremophiles 4*, 83−90.

30. Lesk, A. M., and Chothia, C. (1984) Mechanisms of domain closure in proteins, *J. Mol. Biol. 174*, 175−191.
31. Hayward, S., and Berendsen, H. J. (1998) Systematic analysis of domain motions in proteins from conformational change: new results on citrate synthase and T4 lysozyme, *Proteins 30*, 144−154.
32. Roccatano, D., Mark, A. E., and Hayward, S. (2001) Investigation of the mechanism of domain closure in citrate synthase by molecular dynamics simulation, *J. Mol. Biol. 310*, 1039−1053.
33. Wiegand, G., Remington, S., Deisenhofer, J., and Huber, R. (1984) Crystal structure analysis and molecular model of a complex of citrate synthase with oxaloacetate and S-acetonyl-coenzyme A, *J. Mol. Biol. 174*, 205−219.
34. Pettersson, G., Lill, U., and Eggerer, H. (1989) Mechanism of interaction of citrate synthase with citryl-CoA, *Eur. J. Biochem. 182*, 119−124.
35. Deleted in proof.
36. Cowgill, R. W. (1963) Fluorescence and the structure of proteins. I. Effects of subsitutents on the flurorescence of indole and phenol compounds, *Arch. Biochem. Biophys. 100*, 36−44.
37. Adams, P. D., Chen, Y., Ma, K., Zagorski, M. G., Sonnichsen, F. D., McLaughlin, M. L., and Barkley, M. D. (2002) Intramolecular quenching of tryptophan fluorescence by the peptide bond in cyclic hexapeptides, *J. Am. Chem. Soc. 124*, 9278−9286.
38. Sillen, A., Hennecke, J., Roethlisberger, D., Glockshuber, R., and Engelborghs, Y. (1999) Fluorescence quenching in the DsbA protein from *Escherichia coli*: The complete picture of the excited-state energy pathway and evidence for the reshuffling dynamics of the microstates of tryptophan, *Proteins: Struct., Funct., Genet. 37*, 253−263.
39. Petrich, J. W., Chang, M. C., and Fleming, G. R. (1985) Nonexponential fluorescence decay in tryptophan and tryptophan-containing peptides and proteins, *NATO ASI Ser. 85*, 71−80.
40. Ricci, R. W., and Nesta, J. M. (1976) Inter- and intramolecular quenching of indole fluorescence by carbonyl compounds, *J. Phys. Chem. 80*, 974−980.
41. Chen, Y., Liu, B., Yu, H.-T., and Barkley, M. D. (1996) The peptide bond quenches indole fluorescence, *J. Am. Chem. Soc. 118*, 9271−9278.
42. Chen, Y., and Barkley, M. D. (1998) Toward understanding tryptophan fluorescence in proteins, *Biochemistry 37*, 9976−9982.
43. Ababou, A., and Bombarda, E. (2001) On the involvement of electron transfer reactions in fluorescence decay kinetics heterogeneity of proteins, *Protein Sci. 10*, 2102−2113.
44. Pan, C. P., and Barkley, M. D. (2004) Conformational effects on tryptophan fluorescence in cyclic hexapeptides, *Biophys. J. 86*, 3828−3835.
45. Meech, S. R., Lee, A., and Phillips, D. (1983) On the nature of the fluorescent state of methylated indole derivatives, *Chem. Phys. 80*, 317−328.
46. Vivian, J. T., and Callis, P. R. (2001) Mechanisms of tryptophan fluorescence shifts in proteins, *Biophys. J. 80*, 2093−2109.
47. Callis, P. R., and Vivian, J. T. (2003) Understanding the variable fluorescence quantum yield of tryptophan in proteins using QM-MM simulations. Quenching by charge transfer to the peptide back bone, *Chem. Phys. Lett. 369*, 409−414.
48. Callis, P. R., and Liu, T. (2004) Quantitative prediction of fluorescence quantum yields for tryptophan in proteins, *J. Phys. Chem. B 108*, 4248−4259.
49. Belasco, J. G., and Knowles, J. R. (1980) Direct observation of substrate distortion by triosephosphate isomerase using Fourier transform infrared spectroscopy, *Biochemistry 19*, 472−477.
50. Belasco, J. G., and Knowles, J. R. (1983) Polarization of substrate carbonyl groups by yeast aldolase: investigation by Fourier transform infrared spectroscopy, *Biochemistry 22*, 122−129.
51. Deng, H., Zheng, J., Burgner, J., and Callender, R. (1989) Molecular properties of pyruvate bound to lactate dehydrogenase: a Raman spectroscopic study, *Proc. Natl. Acad. Sci. U.S.A. 86*, 4484−4488.
52. Roberts, M. F., Opella, S. J., Schaffer, M. H., Phillips, H. M., and Stark, G. R. (1976) Evidence from ^{13}C NMR for protonation of carbamyl-P and *N*-(phosphonacetyl)-L-aspartate in the active site of aspartate transcarbamylase, *J. Biol. Chem. 251*, 5976−5985.
53. Tonge, P. J., and Carey, P. R. (1990) Length of the acyl carbonyl bond in acyl-serine proteases correlates with reactivity, *Biochemistry 29*, 10723−10727.
54. Kurz, L. C., Shah, S., Frieden, C., Nakra, T., Stein, R. E., Drysdale, G. R., Evans, C. T., and Srere, P. A. (1995) Catalytic strategy of citrate synthase: subunit interactions revealed as a consequence of a single amino acid change in the oxaloacetate binding site, *Biochemistry 34*, 13278−13288.
55. Simon, E. J., and Shemin, D. (1953) The preparation of *S*-succcinyl coenzyme A, *J. Am. Chem. Soc. 75*, 2520.
56. Lakowicz, J. R. (1999) *Principles of fluorescence spectroscopy*, 2nd ed., Kluwer Academic/Plenum, New York.
57. Chen, R. F. (1967) Fluorescence quantum yields of tryptophan and tyrosine, *Anal. Lett. 1*, 35−42.
58. Sutherland, K. J., Henneke, C. M., Towner, P., Hough, D. W., and Danson, M. J. (1990) Citrate synthase from the thermophilic archaebacterium *Thermoplasma acidophilium*. Cloning and sequencing of the gene, *Eur. J. Biochem. 194*, 839−844.
59. Ridley, J., and Zerner, M. (1973) Intermediate neglect of differential overlap (INDO) technique for spectroscopy: pyrrole and the azines, *Theor. Chim. Acta (Berlin) 32*, 111−134.
60. MacKerell, A. D., Jr., Bashford, D., Bellott, M., Dunbrack, R. L., Evanseck, J. D., Field, M. J., Fischer, S., Gao, J., Ha, S., Joseph-McCarthay, D., Kuchnir, L., Kuczera, K., Lau, F. T. K., Mattos, C., Michnick, S., Ngo, T., Nguyen, D. T., Prodhom, B., Reiher, W. E., III, Roux, B., Schlenkrich, M., Smith, J. C., Stote, R., Straub, J., Watanabe, M., Wiorkiewicz-Kuczera, J., Yin, D., and Karplus, M. (1998) All atom empirical potential for molecular modeling and dynamics studies of proteins, *J. Phys. Chem. B 102*, 3586−3616.
61. Frisch, M. J., Trucks, G. W., Schlegel, H. B., Scuseria, G. E., Robb, M. A., Cheeseman, J. R., Zakrzewski, V. G., Montgomery, J. A., Jr., Stratmann, R. E., Burant, J. C., Dapprich, S., Millam, J. M., Daniels, A. D., Kudin, K. N., Strain, M. C., Farkas, O., Tomasi, J., Barone, V., Cossi, M., Cammi, R., Mennucci, B., Pomelli, C., Adamo, C., Clifford, S., Ochterski, J., Petersson, G. A., Ayala, P. Y., Cui, Q., Morokuma, K., Malick, D. K., Rabuck, A. D., Raghavachari, K., Foresman, J. B., Cioslowski, J., Ortiz, J. V., Stefanov, B. B., Liu, G., Liashenko, A., Piskorz, P., Komaromi, I., Gomperts, R., Martin, R. L., Fox, D. J., Keith, T., Al-Laham, M. A., Peng, C. Y., Nanayakkara, A., Gonzalez, C., Challacombe, M., Gill, P. M. W., Johnson, B. G., Chen, W., Wong, M. W., Andres, J. L., Head-Gordon, M., Replogle, E. S., and Pople, J. A. (1998) *Gaussian 98*, Revision A.11.3, Gaussian, Inc., Pittsburgh, PA.
62. Wikoff, W., Riley, M., Park, J., and Kurz, L. C. (2005) Short strong hydrogen bond in the *Thermoplasma acidophilum* citrate synthase oxaloacetate ternary complex of the intermediate analog, carboxymethyl-coenzyme A: structure of the complex and kinetics of its formation, manuscript in preparation.
63. Russell, R. J., Ferguson, J. M., Hough, D. W., Danson, M. J., and Taylor, G. L. (1997) The crystal structure of citrate synthase from the hyperthermophilic archaeon *Pyrococcus furiosus* at 1.9 Å resolution, *Biochemistry 36*, 9983−9994.
64. Callis, P. R. (1997) ^1L_a and ^1L_b transitions of tryptophan: applications of theory and experimental observations to fluorescence of proteins, *Methods Enzymol. 278*, 113−150.
65. Beechem, J. M., and Brand, L. (1985) Time-resolved fluorescence of proteins, *Annu. Rev. Biochem. 54*, 43−71.
66. Chang, M. C., Petrich, J. W., McDonald, D. B., and Fleming, G. R. (1983) Nonexponential fluorescence decay of tryptophan, tryptophylglycine, and glycyltryptophan, *J. Am. Chem. Soc. 105*, 3819−3824.
67. Karpusas, M., Branchaud, B., and Remington, S. J. (1990) Proposed mechanism for the condensation reaction of citrate synthase: 1.9-Å structure of the ternary complex with oxaloacetate and carboxymethyl coenzyme A, *Biochemistry 29*, 2213−2219.
68. Russell, R. J., Gerike, U., Danson, M. J., Hough, D. W., and Taylor, G. L. (1998) Structural adaptations of the cold-active citrate synthase from an Antarctic bacterium, *Structure 6*, 351−361.
69. Lakowicz, J. R., Joshi, N. B., Johnson, M. L., Szmacinski, H., and Gryczynski, I. (1987) DIffusion coefficients of quenchers in proteins from transient effects in the intensity decays, *J. Biol. Chem 262*, 10907−10910.
70. Eftink, M. R., and Ghiron, C. A. (1976) Fluorescence quenching of indole and model micelle systems, *J. Phys. Chem. 80*, 486−493.
71. Steinberger, R., and Westheimer, F. H. (1951) Metal Ion-catalyzed decarboxylation: A model for an enzyme system, *J. Am. Chem. Soc. 73*, 429−435.
72. Broos, J., Maddalena, F., and Hesp, B. H. (2004) In vivo synthesized proteins with monoexponential fluorescence decay kinetics, *J. Am. Chem. Soc. 126*, 22−23.

73. Gray, H. B., and Winkler, J. R. (1996) Electron transfer in proteins, *Annu. Rev. Biochem. 65*, 537−561.
74. Liang, J., Edelsbrunner, H., and Woodward, C. (1998) Anatomy of protein pockets and cavities: measurement of binding site geometry and implications for ligand design, *Protein Sci. 7*, 1884−1897.
75. Karpusas, M., Holland, D., and Remington, S. J. (1991) 1.9-angstrom structures of ternary complexes of citrate synthase with D- and L-malate: mechanistic implications, *Biochemistry 30*, 6024−6031.
76. Gu, Z. (1996) Mechanism of the condensation reaction of citrate synthase as studied by solid-state NMR, Ph.D. Thesis, Columbia University, New York.

BI048323L